Institute of Space and Aeronautical Science, University of Tokyo
Report No. 430, November 1968

A Theoretical Study for Initiation of High-Frequency Combustion Oscillation in Premixed Gas Rocket

By

Tadao TAKENO

Summary: A theoretical study for initiation of high-frequency combustion oscillation in the premixed gas rocket was conducted. A generalized wave equation which governs the behavior of pressure disturbances in a chemically reacting flow field was derived through the linearization of the fundamental equations. It was shown that the behavior of pressure disturbances depends only on the variation in heat release rate, being independent of the individual chemical reaction processes through which this variation is provided. It was also shown that the equation can be used for the analysis of heat-driven oscillation when the response of heat source to flow disturbances is known. The space conditon for the occurrence of heat-driven oscillation was found to depend upon the way of response of heat source to flow disturbances, while the time condition was found to be independent of it. For the occurrence of high-frequency combustion oscillation in the premixed gas rocket, a simplified analytical model of heat-driven oscillation with an insensitive time delay was postulated on the basis of the previous experimental studies. The incipient amplification rate of the oscillation was calculated as the function of propellant equivalence ratio and combustion chamber length. The calculated oscillation boundary was found to correlate very well with the experimentally observed boundary.

LIST OF SYMBOLS

Superscript *	indicates that the quantity is dimensional
Superscript $'$	indicates a small perturbation
Subscript $_0$	indicates a quantity of stagnant combustion gas at a reference position
Subscript $_1$	indicates a quantity in region I
Subscript $_2$	indicates a quantity in region II
Subscript $_i$	indicates a chemical species i
$-$	over a quantity indicates steady state or mean value
A	interaction index between heat source and flow perturbations
a	thermal diffusivity
B_1	specific admittance ratio of injector
B_2	specific admittance ratio of exhaust nozzle
B_k	a constant in the frequency factor for kth reaction
$\bar{c}_0^*$	sound velocity of stagnant combustion gas at a reference position
c_p	specific heat at constant pressure

c_v	specific heat at constant volume
D	diffusion coefficient
e	specific internal energy of gas mixture
E_k	activation energy for kth reaction
h_i	specific enthalpy of species i
h_i^0	standard heat of formation per unit mass for species i at temperature T^0
L	representative length of analytical system
L_c	combustion chamber length
M	total number of chemical reactions occurring
m	zero or positive integer indicating number of oscillation periods contained in critical time delay
N	total number of chemical species present
n	positive integer indicating oscillation mode
p	hydrostatic pressure
$\boldsymbol{P}$	pressure tensor
q	heat release rate of gas mixture per unit volume
$\boldsymbol{q}$	heat flux vector
R	gas constant of mixture
R^0	universal gas constant
$\boldsymbol{r}$	position vector
$s=\alpha+i\beta$	complex frequency
s_0	acoustical resonant frequency of analytical system
T	temperature or period of oscillation
T^0	a fixed standard reference temperature
t	time
u	axial component of velocity
$\boldsymbol{v}$	velocity vector
V_i	diffusion velocity vector of species i
$\overline{W}$	average molecular weight of mixture
W_i	molecular weight of species i
w_i	rate of production of species i by chemical reaction
X_i	mole fraction of species i
x	axial distance
Y_i	mass fraction of species i
α	real part of s or amplification rate of oscillation
α_k	exponent determining temperature dependence of the frequency factor for kth reaction
β	imaginary part of s or angular frequency of oscillation
γ	specific heat ratio
κ	bulk viscosity coefficient
λ	thermal conductivity
μ	coefficient of viscosity

ν	kinematic viscosity
$\nu'_{i,k}$	stoichiometric coefficient for species i appearing as a reactant in kth reaction
$\nu''_{i,k}$	stoichiometric coefficient for species i appearing as a product in kth reaction
ξ	axial distance of plane heat source
ρ	density
τ	response time delay
τ_c	critical value of response time delay for neutral oscillation
φ	propellant equivalence ratio
ω	critical value of angular frequency for neutral oscillation
$F(z)$	arbitrary function of arguement z defining downstream propagating pressure waves
$f(z)$	arbitrary function of arguement z defining upstream propagating pressure waves
$Q_\xi(t)$	function of time defined by Eq. (4-1)
$\Omega(\xi)$	function of position of plane heat source defined by Eq. (4-19)
$\delta(x)$	Dirac delta function
$\nu(x)$	time independent part of u'
$\sigma(x)$	time independent part of p'

1. Introduction

An investigation on the high-frequency combustion oscillation of the longitudinal mode has been conducted by the present author by using a rocket motor which burns the premixed gas as the propellant. The objects of the investigation are to make clear the essential natures and the initiating and driving mechanism of the oscillation through experiments, and then to develop a theory which can explain quantitatively the occurrence of the oscillation. The initial phase of the investigation [*1*],[*2*] has elucidated the phenomenological aspect of the oscillation. The observed pressure oscillations of the fundamental, the second harmonic, and the third harmonic mode were characterized by the presence of pressure waves of finite amplitude propagating back and forth in the combustion chamber. The pressure waves were sinusoidal-type waves of small amplitude near the instability boundary, but they were always shock-type waves of large amplitude in the instability region. In the experiments, the existence of an upper critical chamber length, as well as that of a lower critical chamber length, was observed. Any given mode of oscillation occurred only between these two critical chamber lengths. A detailed examination of the data has led to a conclusion that the occurrence of the oscillation is governed by a certain characteristic time.

The second phase of the investigation [*3*] has made clear that the shock-type pressure oscillation excited in the chamber is essentially an acoustic standing pressure oscillation of smooth sinusoidal waveform, although the observed pressure wave-

form exhibited a peculiar shock-type waveform as if a substantial shock wave were propagating in the chamber. It was found that a small pressure pulse is propagating back and forth in the chamber being superimposed on the sinusoidal standing wave oscillation, which gives rise to the peculiar pressure waveform. The propagation of the pulse in the chamber was isentropic except at the flame zone concentrated near the injector end. The shock wave did not play so important role as was expected from the observed pressure waveform.

The third phase of the investigation [4] has brought about the following conclusions on the driving mechanism of the oscillation. The excited standing pressure oscillation is a kind of heat-driven oscillation, in which the variation in heat release rate at the flame zone drives the standing pressure oscillation in the chamber. The increase in heat release rate is provided by the periodical spontaneous ignitions of the unburnt propellant volumes. These volumes are thrown out in the hot combustion gas stream from the turbulent multiflames stabilized near the injector end, on account of the flame tip breaking. This breaking is caused as the result of the rapid increase of the propellant injection velocity into the chamber. The latter, in turn, is caused by the standing pressure oscillation in the chamber, and thus closes the cycle of the self-excited oscillation. The characteristic time which governs the occurrence of the oscillation is identified as the response time delay of the unburnt propellant, the substance of which is the ignition time delay of the thrown out propellant in the hot turbulent combustion gas stream.

The object of the present study, which constitutes the fourth and final phase of the investigation, is to develop on the basis of the so far obtained experimental findings a theory which can explain quantitatively the occurrence of the oscillation. The important results obtained through the whole investigation, as well as the significance of the gas rocket, will also be discussed.

2. Historical Survey

Theoretical studies on the high-frequency combustion oscillation in the premixed gas rocket have been performed by several investigators [6]~[8]. In those theories, the driving mechanism of the oscillation depends upon the chemical kinetic factors. The previous studies [4] of the present author, however, has made clear that it is the complicated fluid dynamic influences, instead of the chemical kinetic factors, that actually play an important role in the driving of the oscillation. It has been concluded that the theories based on the chemical kinetics model are invalid for describing the oscillation in the gas rocket. The sensitive time lag theory [9] also, which was developed for the high-frequency combustion oscillation in the liquid propellant rocket, cannot be applied to the gas rocket. In the theory, the combustion process is replaced by a mass source spouting out the combustion gas, and the driving force of the oscillation is provided by the increased mass addition of the source in response to the pressure perturbation. In a sense, the excited oscillation postulated in the theory should be called "mass-driven oscillation". In the gas rocket, on the other hand, it is the energy or heat addition rather than the mass addition, which

actually drives the oscillation. It should also be noticed that the response time delay in the driving mechanism suggested in the previous studies [4] is insensitive to the flow disturbances in each cycle of the oscillation. It can be concluded, therefore, that none of the theories developed so far can correctly explain the occurrence of the oscillation in the gas rocket. The correct theory, as was pointed out in the previous studies [4], should be based on the driving mechanism which depends upon the interaction between pressure waves and flames.

On the other hand, the heat-driven oscillation with a constant (insensitive) time lag has been analyzed by Blackshear [10],[11], with the object of revealing the important parameters which control the ability of a flame to drive or damp an imposed oscillation. The reflection, transmission, and amplification of pressure waves passing through a laminar flame region were determined by applying the continuity and the momentum equations over the flame region. It was shown that a change in flame area acts as a source of waves propagating simultaneously into the hot and the cold gases on either side of the flame zone. Bailey [12] developed a theory for the instability of a flat flame, in which the driving force of the oscillation is provided by the variation of the burning velocity. Merk [13]~[17] has performed a series of detailed analyses of the heat-driven oscillation. The general characteristic equation governing the occurrence of the oscillation was derived from the energy and the momentum equations applied across the heat source. In the equation, the transfer function of the heat source is introduced, which describes the response of the source to perturbations in the flow and thermodynamic variables in the gas flow.

In those theories of the heat-driven oscillation, the dynamic stability of the flow system depends mainly upon the interaction between the heat source and the flow disturbances. It is necessary, therefore, to examine this interaction problem, especially that of flame and pressure wave, before the analysis of the combustion oscillation in the gas rocket. This problem has been studied by numbers of investigators, and the extensive literatures have been reviewed by Markstein [18]. When a pressure wave interacts with a flame, it creates a system of transmitted and reflected waves while the initial shape of the flame is distorted. In general, the effective flame front area is increased and the resulting increased heat release rate of combustion is accompanied by emission of further pressure waves. While the initially reflected and transmitted waves are almost instantaneously established, the waves that are caused by the deformation of the flame area are emitted with some time delay. The experimental observations show the complexity of the interaction phenomenon and thereby illustrate the difficulties of the theoretical analysis.

Chu [19]~[21] studied theoretically the mechanism of generation of pressure waves at the flame front. He showed that the pressure wave will be generated at the flame front whenever there is a change in the rate of heat release. The change may be caused as a result of changes in the burning velocity, density, or heating value, and so forth. The strength of the generated pressure wave depends only upon the change in heat release rate, being independent of how such change is produced. Ruddinger [22] studied the interaction of shock or other pressure waves with a plane flame front as part of a general nonsteady flow system by the wave diagram pro-

cedures. He showed how the calculations can be carried out, if the effects of flow perturbations on the burning velocity and the heating value are known.

The above survey suggests an idea that in the study of the interaction problem between flame and flow field, we should distinguish between two aspects of the problem: first, the dynamic effects of heat release on flow field, and second, the response of flame to flow disturbances. In the present study, these two aspects will be treated separately. The first aspect of the problem is rather easy to solve, since the dynamic effects of a given amount of heat release can be determined completely through the theories of thermodynamics and gasdynamics without any knowledge of chemical reaction. In the previous studies of heat-driven oscillation [*10*]~[*17*], only two of three (mass, momentum, and energy) conservation equations were used. However, the accurate prediction of the dynamic effects can only be made by the simultaneous use of three conservation equations with equation of state, without any unnecessary assumptions. The second aspect is very difficult to solve theoretically, although it is more important from the point of view of basic combustion theory. In order to obtain the accurate theoretical prediction of flame response to flow disturbances, the internal structure of flame itself should be known, and hence the detailed knowledges of chemical reaction process, as well as those of transport properties, are required. This is almost impossible even in the simplest case of the one dimensional laminar flame. When the combustion proceeds through the turbulent multiflames, as is the case of the present investigation, the accurate prediction by theory seems out of question. The simplifying assumptions, which are necessary to make the analysis possible, will inevitably make the model far from the actual phenomenon, and thus the analysis will have no physical significances. Therefore, the mathematical representation of the flame response is obliged to be an empirical one based on the experimental findings.

In the present theoretical study, a generalized wave equation for the multicomponent reacting gas mixtures will be derived first, so as to determine the dynamic effect of chemical reaction on flow field. The derivation is somewhat similar to those of Chu [*20*] and Culick [*7*], but is more general since the effect of chemical reaction as well as of transport phenomena is considered. It will be shown that the chemical reaction affects the flow field only through the variation in heat release rate, being independent of the individual chemical reaction processes through which the variation is provided. The wave equation is used to show how the pressure oscillation is excited in the flow system when there is a variation in heat release rate in the system. An empirical relation based on the experimental findings is introduced for the response of flames, or heat source, to flow disturbances. The relation is used for obtaining the characteristic equation which determines the incipient stability of the postulated analytical system for the gas rocket.

3. Dynamic Effect of Chemical Reaction on Flow Field

3-1. *Governing Equations*

In order to analyze the dynamic effect of chemical reaction on flow field, the fol-

lowing six assumptions are made.

1. The reacting gas mixture behaves like an ideal gas.
2. The transport coefficients such as the coefficient of viscosity, the thermal conductivity, and the diffusion coefficient are the same for all chemical species and constant.
3. The effect of pressure diffusion, as well as that of thermal diffusion, can be neglected.
4. The specific heat at constant pressure is the same for all chemical species and depends only on temperature.
5. The average molecular weight of the mixture does not change and remains constant in the course of chemical reaction.
6. There are no external forces.

With these assumptions, the multicomponent reacting ideal gas mixtures are governed by the following equations [*23*].

Over all continuity equation:

$$\frac{\partial \rho^*}{\partial t^*} + \nabla^* \cdot (\rho^* \boldsymbol{v}^*) = 0. \tag{3-1}$$

Momentum equation:

$$\rho^* \frac{\partial \boldsymbol{v}^*}{\partial t^*} + \rho^* \boldsymbol{v}^* \cdot \nabla^* \boldsymbol{v}^* = -\nabla^* \cdot \boldsymbol{P}^*. \tag{3-2}$$

Energy equation:

$$\rho^* \frac{\partial e^*}{\partial t^*} + \rho^* \boldsymbol{v}^* \cdot \nabla^* e^* = -\nabla^* \cdot \boldsymbol{q}^* - \boldsymbol{P}^* : (\nabla^* \boldsymbol{v}^*). \tag{3-3}$$

Continuity equation for each species:

$$\rho^* \frac{\partial Y_i}{\partial t^*} + \rho^* \boldsymbol{v}^* \cdot \nabla^* Y_i = w_i^* - \nabla^* \cdot (\rho^* Y_i V_i^*), \quad i = 1, 2, \cdots, N. \tag{3-4}$$

Equation of state:

$$p^* = \rho^* R^* T^*, \tag{3-5}$$

where $R^* = R^{0*} / \overline{W}^*$ is the gas constant for the mixture. In Eqs. (3-2) and (3-3), $\boldsymbol{P}^*$ is given by

$$\boldsymbol{P}^* = \left\{ p^* + \left(\frac{2}{3} \mu^* - \kappa^* \right) (\nabla^* \cdot \boldsymbol{v}^*) \right\} \boldsymbol{U} - \mu^* [(\nabla^* \boldsymbol{v}^*) + (\nabla^* \boldsymbol{v}^*)^T], \tag{3-6}$$

and in Eq. (3-3) $\boldsymbol{q}^*$ is given by

$$\boldsymbol{q}^* = -\lambda^* \nabla^* T^* + \rho^* \sum_{i=1}^{N} h_i^* Y_i V_i^*. \tag{3-7}$$

In Eqs. (3-1) through (3-7), vector notation is employed, ∇^* is the gradient operator, the tensor $\nabla^* \boldsymbol{v}^*$ is a derivative operator, $\boldsymbol{U}$ is the unit tensor, two dots (:) imply that the tensors are to be contracted twice, and superscript ^{T} denotes the transpose of the tensor.

The $N+6$ dependent variables in Eqs. (3-1) through (3-5) may be taken to be p^*, ρ^*, T^*, $\boldsymbol{v}^*$ and Y_i, in which case the other variables may be related to these

through the diffusion equation

$$Y_i V_i^* = -D^* \nabla^* Y_i, \quad i=1, 2, \cdots, N, \tag{3-8}$$

the thermodynamic identity

$$e^* = \sum_{i=1}^{N} h_i^* Y_i - p^*/\rho^*, \tag{3-9}$$

the carolic equation of state

$$h_i^* = h_i^{0*} + \int_{T^{0*}}^{T^*} c_p^* dT^*, \quad i=1, 2, \cdots, N, \tag{3-10}$$

and the phenomenological chemical kinetic expression

$$w_i^* = W_i^* \sum_{k=1}^{M} (\nu''_{i,k} - \nu'_{i,k}) B_k^* T^{*\alpha_k} e^{-(E_k^*/R^{0*}T^*)} \prod_{j=1}^{N} \left(\frac{X_j p^*}{R^{0*} T^*} \right)^{\nu'_{j,k}}$$
$$i=1, 2, \cdots, N. \tag{3-11}$$

The following Eqs. (3-12) through (3-15) comprise subsidiary relationships that are required in the analysis.

$$\sum_{i=1}^{N} Y_i = 1. \tag{3-12}$$

$$X_i = \overline{W}^* \frac{Y_i}{W_i^*}, \quad i=1, 2, \cdots, N. \tag{3-13}$$

$$\sum_{i=1}^{N} Y_i V_i^* = 0. \tag{3.14}$$

$$\sum_{i=1}^{N} w_i^* = 0. \tag{3-15}$$

In order to elucidate the effect of chemical reaction, another form of the energy equation will be used in the present analysis. In view of Eqs. (3-9), (3-10) and (3-12), the specific internal energy e^* of the gas mixture may be written as

$$e^* = \sum_{i=1}^{N} Y_i h_i^{0*} + \int_{T^{0*}}^{T^*} c_p^* dT^* - p^*/\rho^*. \tag{3-16}$$

Substituting this expression and Eqs. (3-4) and (3-7) into Eq. (3-3), we obtain

$$\rho^* \frac{D}{Dt^*} \left(\int_{T^{0*}}^{T^*} c_p^* dT^* - \frac{p^*}{\rho^*} \right) = -\sum_{i=1}^{N} h_i^{0*} w_i^* + \lambda^* \nabla^{*2} T^* - \boldsymbol{P}^* : (\nabla^* \boldsymbol{v}^*), \tag{3-17}$$

since

$$\rho^* \sum_{i=1}^{N} (h_i^{0*} - h_i^*) Y_i V_i^* = -\rho^* \int_{T^{0*}}^{T^*} c_p^* dT^* \sum_{i=1}^{N} Y_i V_i^* = 0,$$

according to Eq. (3-14). In Eq. (3-17), the substantial derivative $\frac{D}{Dt^*}$ is defined by

$$\frac{D}{Dt^*}=\frac{\partial}{\partial t^*}+\boldsymbol{v}^*\cdot\nabla^*.$$

From Eq. (3-5) it can be shown that

$$\int_{T^{0*}}^{T^*}c_p^*dT^*-p^*/\rho^*=\int_{T^{0*}}^{T^*}c_p^*dT^*-R^*\int_{T^{0*}}^{T^*}dT^*-R^*T^{0*}$$
$$=\int_{T^{0*}}^{T^*}c_v^*dT^*-R^*T^{0*},$$

where $c_v^*=c_p^*-R^*$ is the constant depending only on temperature. Substituting the above relation into Eq. (3-17), we obtain

$$\rho^*\frac{D}{Dt^*}\left(\int_{T^{0*}}^{T^*}c_v^*dT^*\right)=-\sum_{i=1}^{N}h_i^{0*}w_i^*+\lambda^*\nabla^{*2}T^*-\boldsymbol{P}^*:(\nabla^*\boldsymbol{v}^*),\qquad(3\text{-}18)$$

for the energy equation.

For simplicity, we assume here that there exists the average value $\bar{c}_v^*$ which is independent of temperature. Then

$$\int_{T^{0*}}^{T^*}c_v^*dT^*=\bar{c}_v^*(T^*-T^{0*}).\qquad(3\text{-}19)$$

Substituting this into Eq. (3-18), we finally obtain

$$\bar{c}_v^*\rho^*\frac{\partial T^*}{\partial t^*}+\bar{c}_v^*\rho^*\boldsymbol{v}^*\cdot\nabla^*T^*=-\sum_{i=1}^{N}h_i^{0*}w_i^*+\lambda^*\nabla^{*2}T^*-\boldsymbol{P}^*:(\nabla^*\boldsymbol{v}^*).\qquad(3\text{-}20)$$

Equations (3-1), (3-2), and (3-20) may be taken to be the governing differential conservation equations. When the chemical reaction takes place in the flow field, w_i^* may be considered as given and these equations together with the equation of state (3-5) form a system of six equations which govern the six unknowns p^*, ρ^*, T^*, and $\boldsymbol{v}^*$.

For convenience, the governing equations are expressed in terms of the dimensionless quantites. We select as the reference time t_0^* the time required for a sound wave to travel a distance L (representative length) under the conditions corresponding to the stagnant combustion gas at a reference position. If the sound velocity in the stagnant combustion gas is denoted as $\bar{c}_0^*$, then $t_0^*=L/\bar{c}_0^*$. We express the velocity $\boldsymbol{v}^*$ as a fraction of $\bar{c}_0^*$ and write $\boldsymbol{v}=\boldsymbol{v}^*/\bar{c}_0^*$. Likewise, the pressure, density, and temperature of the combustion gas at the stagnant condition will be taken as reference quantities. For the standard heat of formation h_i^{0*} and the production rate w_i^* of each species, $\bar{e}_0^*$ and $\bar{w}_0^*$ defined by the following equations are taken as reference quantities. Thus the dimensionless time, position, velocity, pressure, density, temperature, and heat of formation and production rate of species i are defined as:

$$t=\frac{t^*}{t_0^*},\quad \boldsymbol{r}=\frac{\boldsymbol{r}^*}{L},\quad \boldsymbol{v}=\frac{\boldsymbol{v}^*}{\bar{c}_0^*},\quad p=\frac{p^*}{\bar{p}_0^*},\quad \rho=\frac{\rho^*}{\bar{\rho}_0^*},$$
$$T=\frac{T^*}{\bar{T}_0^*},\quad h_i^0=\frac{h_i^{0*}}{\bar{e}_0^*},\quad w_i=\frac{w_i^*}{\bar{w}_0^*},\qquad(3\text{-}21)$$

where

$$\bar{e}_0^* = \bar{c}_v^* \bar{T}_0^*, \quad \bar{w}_0^* = \frac{\bar{\rho}_0^*}{t_0^*}.$$

Superscript $^-$ over a quantity indicates steady state value.

With these dimensionless quantities, the governing equations can be rewritten in the following form.

$$\frac{\partial \rho}{\partial t} + \nabla \cdot (\rho \boldsymbol{v}) = 0, \tag{3-22}$$

$$\rho \frac{\partial \boldsymbol{v}}{\partial t} + \rho \boldsymbol{v} \cdot \nabla \boldsymbol{v} = -\frac{1}{\gamma} \nabla \cdot \boldsymbol{P}, \tag{3-23}$$

$$\rho \frac{\partial T}{\partial t} + \rho \boldsymbol{v} \cdot \nabla T = -\sum_{i=1}^{N} h_i^0 w_i + a \nabla^2 T - (\gamma - 1)(\boldsymbol{P} : \nabla \boldsymbol{v}), \tag{3-24}$$

$$p = \rho T, \tag{3-25}$$

where ∇ is the dimensionless gradient operator and γ is the specific heat ratio defined by $\gamma = \bar{c}_p^* / \bar{c}_v^*$. The dimensionless pressure tensor $\boldsymbol{P}$ is defined by

$$\boldsymbol{P} = \left\{ p + \left(\frac{2}{3} \nu - \kappa \right) (\nabla \cdot \boldsymbol{v}) \right\} \boldsymbol{U} - \nu \{ (\nabla \boldsymbol{v}) + (\nabla \boldsymbol{v})^T \}, \tag{3-26}$$

while the dimensionless transport coefficients ν, κ, and a are defined by

$$\nu = \gamma \frac{\mu^* / \bar{\rho}_0^*}{L^2 / t_0^*}, \quad \kappa = \gamma \frac{\kappa^* / \bar{\rho}_0^*}{L^2 / t_0^*}, \quad a = \frac{\lambda^* / (\bar{c}_v^* \bar{\rho}_0^*)}{L^2 / t_0^*}. \tag{3-27}$$

3-2. *Generalized Wave Equation*

For the analysis of small perturbations in the flow field, the unsteady gas flow will be considered as consisting of a small perturbation superposed on the steady state or mean flow. For any dependent variable f appearing in the governing equations, we shall set $f = \bar{f} + f'$ where $\bar{f}$ is a steady state value depending only on position $\boldsymbol{r}$ and f' is small. The expressions are substituted into Eqs. (3-22) through (3-25), and the perturbations are assumed to be so small that the squares and the products of these perturbations and their derivatives can be neglected as compared to terms linear in these perturbations. In addition to this assumption, an important assumption will be introduced here. The steady state flow velocity is assumed to be so small as compared to the sound velocity of the stagnant combustion gas that $\boldsymbol{v}$ is the same order with perturbations, and hence the products with perturbations and their derivatives can be neglected.

The equations governing the steady state flow can easily be obtained from Eqs. (3-22) through (3-25).

$$\nabla \cdot (\bar{\rho} \bar{\boldsymbol{v}}) = 0, \tag{3-28}$$

$$\nabla \cdot \bar{\boldsymbol{P}} = 0, \tag{3-29}$$

$$\bar{\rho}\bar{\boldsymbol{v}}\cdot\nabla\bar{T}=-\sum_{i=1}^{N}h_i^0\bar{w}_i+a\nabla^2\bar{T}-(\gamma-1)(\bar{\boldsymbol{P}}:\nabla\bar{\boldsymbol{v}}), \tag{3-30}$$

$$\bar{p}=\bar{\rho}\bar{T}, \tag{3-31}$$

where the steady state pressure tensor is defined as

$$\bar{\boldsymbol{P}}=\left\{\bar{p}+\left(\frac{2}{3}\nu-\kappa\right)(\nabla\cdot\bar{\boldsymbol{v}})\right\}\boldsymbol{U}-\nu\{(\nabla\bar{\boldsymbol{v}})+(\nabla\bar{\boldsymbol{v}})^T\}. \tag{3-32}$$

On the other hand, the following linearized equations are obtained for the non-steady perturbations.

$$\frac{\partial\rho'}{\partial t}+\nabla\cdot(\bar{\rho}\boldsymbol{v}')=0, \tag{3-33}$$

$$\bar{\rho}\frac{\partial\boldsymbol{v}'}{\partial t}+\frac{1}{\gamma}\nabla\cdot\boldsymbol{P}'=0, \tag{3-34}$$

$$\bar{\rho}\frac{\partial T'}{\partial t}+\bar{\rho}\boldsymbol{v}'\cdot\nabla\bar{T}=-\sum_{i=1}^{N}h_i^0w_i'+a\nabla^2T'-(\gamma-1)(\bar{\boldsymbol{P}}:\nabla\boldsymbol{v}'), \tag{3-35}$$

$$p'=\rho'\bar{T}+\bar{\rho}T', \tag{3-36}$$

where the pressure tensor for the perturbation is defined as

$$\boldsymbol{P}'=\left\{p'+\left(\frac{2}{3}\nu-\kappa\right)(\nabla\cdot\boldsymbol{v}')\right\}\boldsymbol{U}-\nu\{(\nabla\boldsymbol{v}')+(\nabla\boldsymbol{v}')^T\}. \tag{3-37}$$

Equations (3-29), (3-32), (3-33) and (3-36) can be used to reduce the energy equation (3-35) to

$$\frac{\partial p'}{\partial t}=-\gamma\bar{p}\nabla\cdot\boldsymbol{v}'-\sum_{i=1}^{N}h_i^0w_i'+a\nabla^2T'. \tag{3-38}$$

We make use of this equation and Eq. (3-34) to obtain a single partial differential equation for the pressure perturbation,

$$\frac{\partial^2p'}{\partial t^2}=\bar{p}\nabla\cdot\left(\frac{1}{\bar{\rho}}\nabla\cdot\boldsymbol{P}'\right)-\sum_{i=1}^{N}\left(h_i^0\frac{\partial w_i'}{\partial t}\right)+a\nabla^2\left(\frac{\partial T'}{\partial t}\right). \tag{3-39}$$

Equation (3-39) governs the behavior of the pressure perturbation in the multi-component reacting gas mixtures. However, we should mention that even for simple one dimensional flow system, to solve the equation is a very complicated task. In order to obtain a more simple form of equation, we shall proceed to make additional assumption that the magnitudes of the dimensionless transport coefficients ν, κ, and a are the same order with the perturbations. Although the assumption limits the range of applicability of the equation, the resulting equation nevertheless remain valid in a reasonable approximation for many problems of the combustion oscillation. In fact, if we take the combustion chamber length as the representative length L, these coefficients becomes less than 10^{-4} for a representative case. This simply illustrates the fact that the transport phenomena occur so slowly as compared to the sound wave propagation, that they are unimportant in the problem of the

combustion oscillation.

According to the above assumption, Eqs. (3-32) and (3-37) reduce to

$$\bar{\boldsymbol{P}}=\bar{p}\boldsymbol{U}=\bar{p}, \qquad \boldsymbol{P}'=p'\boldsymbol{U}=p', \tag{3-40}$$

and hence

$$\nabla\cdot\bar{\boldsymbol{P}}=\nabla\bar{p}, \qquad \nabla\cdot\boldsymbol{P}'=\nabla p'. \tag{3-41}$$

From Eq. (3-29), we obtain

$$\nabla\bar{p}=0,$$

and therefore

$$\bar{p}=\text{const.}=1.0. \tag{3-42}$$

Equation (3-31) reduces to

$$\bar{\rho}\bar{T}=1.0. \tag{3-43}$$

Substituting Eqs. (3-41) through (3-43) into Eq. (3-39), we finally obtain

$$\frac{\partial^2 p'}{\partial t^2}=\nabla\cdot(\bar{T}\nabla p')+\frac{\partial q'}{\partial t}, \tag{3-44}$$

where the variation in heat release rate q' due to chemical reaction is defined as

$$q'=-\sum_{i=1}^{N} h_i^0 w_i'. \tag{3-45}$$

Equation (3-44) is a generalized wave equation in the sense that it includes the term due to the variation in chemical reaction rate as well as the usual acoustic terms. The equation will govern the behavior of pressure wave in the flow field accompanied by the chemical reaction, and should be used as the fundamental equation for the analysis of the combustion oscillation. It can be seen that whenever there is a change in chemical reaction rate there will be always pressure waves generated. It should be noticed that the behavior of pressure waves depends only on the variation in heat release rate. The individual chmical reaction processes, through which this variation is provided, do not affect explicitly the pressure wave but affect implicitly through the variation in total heat release rate.

4. Analysis of Heat-Driven Oscillation

4-1. *One Dimensional Analytical Model*

The generalized wave equation (3-44) can be used to determine the behavior of pressure perturbations in any flow field accompanied by heat addition, so long as the steady state flow velocity is small as compared with the sound velocity. Although the perturbation in heat release rate q' defined by Eq. (3-45) is the one due to chemical reaction, it is not difficult to show that the same equation equally applies to the case when q' is provided by any other means [5]. The equation, therefore, can be used as the fundamental equation of the heat-driven oscillation. However, for the analysis of the complicated nonsteady combustion phenomenon of the pres-

ent investigation, some additional approximations are inevitably required. These approximations made here may be valid only in the particular case of the present investigation, but the general treatment of the analysis can be applied to any other cases of heat-driven oscillation.

As has been made clear in the so far conducted experimental studies of the present investigation, the observed pressure oscillation has definite one dimensional characters. Therefore, the incipient instability of the gas rocket may be studied by the one dimensional linear theory, if we can give a proper one dimensional representation for the complex three dimensional interaction phenomenon between pressure waves and flames. In usual one dimensional analyses of flame-driven oscillation [10]~[17], a flame zone of zero or finite thickness which separates the unburnt gas region from that of the burnt gas is assumed to exist. However, when the combustion proceeds through turbulent multiflames as is the case of the present investigation, most of the combustion region is occupied by the recirculating hot combustion gas [*4*]. The unburnt gas surrounded by the flames occupies only a small portion of the combustion region. The reflection, transmission, and dispersion of pressure waves at the flames will affect little the overall one dimensional character of the propagating pressure waves. In the present analysis, therefore, the existence of the flames, as well as that of the unburnt gases inside the flames, is assumed to be neglected with regard to the one dimensional wave propagation. Everywhere in the chamber is occupied by the hot combustion gas, which flows from the injector toward the exhaust nozzle with a slow flow velocity. There is no steady state combustion zone in the chamber and the flames manifest their effects only in the form of the variation in heat release rate at a fixed one dimensional heat source zone, which is assumed to exist at the position of multiflame tips.

As was described in the previous paper [*3*], there exists in the actual combustion chamber a slight temperature gradient of the combustion gas along the flow direction. However, the gradient of steady state temperature has no important influence upon the stability of the pressure wave in the chamber, although some correction of the wave propagation time may be required. In the present analysis, therefore, $\bar{T}(x)$ is assumed to be constant through the chamber and is taken as unity. Then the steady state density $\bar{\rho}(x)$ also becomes unity from Eq. (3-43). The propagation of the pressure wave in the combustion chamber is isentropic [*3*] except at the heat source zone, where the variation in heat release rate occurs. Some of the energy of the pressure oscillation in the chamber may be lost at the injector end, as well as at the exhaust nozzle end. The magnitude of the energy loss can be represented by the specific admittance ratio B at these ends, which is defined by $B=\gamma u'/p'$.

With these assumptions made above, the actual combustion chamber can be replaced by the hypothetical chamber represented in Fig. 1. The representative length L in this case is the chamber length. The hypothetical injector which admits the steady state flow of hot combustion gas is located at $x=0$, while the hypothetical exhaust nozzle for ejection of the steady state flow is located at $x=1.0$. The reflection of the pressure wave at the injector and the nozzle is specified by the respective admittance ratio. The chamber may be divided conveniently into three zones,

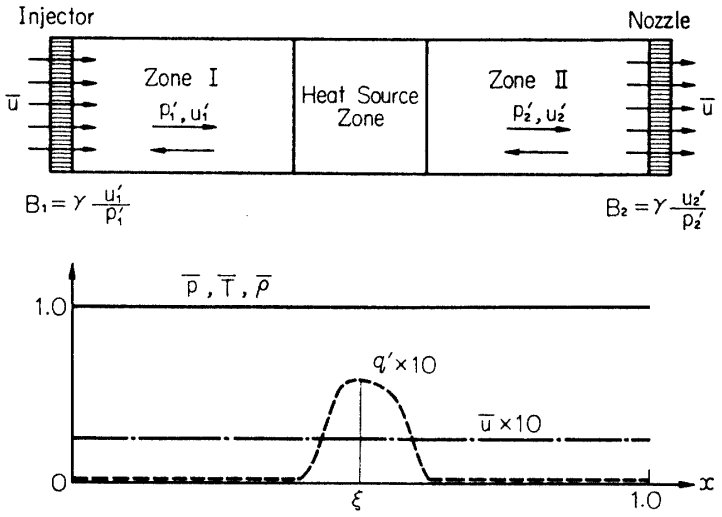

FIG. 1. Nondimensional analytical model of heat-driven oscillation.

namely into the zone I, the zone II, and the heat source zone. In the zones I and II the propagation of the pressure wave is isentropic, while at the heat source zone the variation of heat release rate occurs.

4-2. *Forced Oscillation by Heat Relase*

Before the analysis of the incipient stability, let us first examine the behavior of the postulated hypothetical system when a periodic heat release rate is applied. To obtain the solution of Eq. (3-44) for a heat release rate q' of arbitrary form, we first examine the case when q' is concentrated at $x=\xi$. In this case, q' is given by

$$q'=Q_\xi(t)\,\delta(x-\xi), \tag{4-1}$$

where $Q_\xi(t)$ is a reasonable known function of t, and $\delta(x)$ is the Dirac delta function of x.

The wave equation (3-44) for the zones I and II is reduced to the usual acoustic wave equation

$$\frac{\partial^2 p'}{\partial t^2}=\frac{\partial^2 p'}{\partial x^2}. \tag{4-2}$$

The velocity perturbation u' is related to p' through the following equation which is obtained from the momentum equation (3-34),

$$\frac{\partial u'}{\partial t}+\frac{1}{\gamma}\frac{\partial p'}{\partial x}=0. \tag{4-3}$$

The general solution of Eq. (4-2) is given by

$$p'=f(x+t)+F(x-t), \tag{4-4}$$

where f and F are arbitrary functions defining the upstream and the downstream propagating pressure waves. The corresponding velocity perturbation can be obtained by Eq. (4-3) as

$$u'=-\frac{1}{\gamma}\{f(x+t)-F(x-t)\}. \tag{4-5}$$

These solutions apply equally well in the zones I and II. Let subscript $_1$ denote solutions in the zone I and subscript $_2$ denote solutions in the zone II.

The solutions in the zone I must satisfy the boundary condition at $x=0$,

$$\gamma\frac{u_1'}{p_1'}=B_1, \tag{4-6}$$

where B_1 is the complex specific admittance ratio of the injector. From this condition, we get

$$F_1(z)=\frac{1+B_1}{1-B_1}f_1(-z), \tag{4-7}$$

where z is an arbitrary argument. Substituting this into Eqs. (4-4) and (4-5), we obtain

$$p_1'=f_1(x+t)+\frac{1+B_1}{1-B_1}f_1(-x+t), \tag{4-8}$$

$$u_1'=-\frac{1}{\gamma}\left\{f_1(x+t)-\frac{1+B_1}{1-B_1}f_1(-x+t)\right\}. \tag{4-9}$$

The solutions in the zone II must satisfy the boundary condition at $x=1.0$,

$$\gamma\frac{u_2'}{p_2'}=B_2, \tag{4-10}$$

where B_2 is the complex specific admittance ratio of the nozzle. From this condition, we get

$$F_2(z)=\frac{1+B_2}{1-B_2}f_2(2-z). \tag{4-11}$$

Substituting this into Eqs. (4-4) and (4-5), we get

$$p_2'=f_2(x+t)+\frac{1+B_2}{1-B_2}f_2(2-x+t), \tag{4-12}$$

$$u_2'=-\frac{1}{\gamma}\left\{f_2(x+t)-\frac{1+B_2}{1-B_2}f_2(2-x+t)\right\}. \tag{4-13}$$

The above obtained two sets of solutions are to be matched at the heat source zone, the width of which is assumed here to be zero. Since the governing differential equations in the zones I and II are second order, two matching conditions are required at this heat source plane, in addition to the above two boundary conditions. This plane is characterized by the finite evolution of heat and the dynamic effect of which should be determined by Eq. (3-44). The latter, in the present case, reduces to

$$\frac{\partial^2 p'}{\partial t^2}=\frac{\partial^2 p'}{\partial x^2}+\frac{\partial}{\partial t}Q_\xi(t)\delta(x-\xi). \tag{4-14}$$

The first matching condition can be obtained by integrating the above equation over the infinitesimal reaction zone width, and then making use of Eq. (4-3). The second condition can be obtained by repeating twice the integration. The results are

$$\gamma(u_2'-u_1')=Q_\xi(t), \tag{4-15}$$

$$p_1'=p_2'. \tag{4-16}$$

Equations (4-15) and (4-16) indicate that the finite evolution of heat at the plane heat source will produce the velocity jump across the plane, while the pressure is continuous at any instant across the plane. When Eqs. (4-8), (4-9), (4-12), and (4-13) are substituted into the above two conditions, the following two equations are obtained.

$$\frac{1}{1-B_1}[f_1(\xi+t)+f_1(-\xi+t)-B_1\{f_1(\xi+t)-f_1(-\xi+t)\}]$$
$$-\frac{1}{1-B_2}[f_2(\xi+t)+f_2(2-\xi+t)+B_2\{f_2(2-\xi+t)-f_2(\xi+t)\}]=0, \tag{4-17}$$

$$\frac{1}{1-B_1}[f_1(\xi+t)-f_1(-\xi+t)-B_1\{f_1(\xi+t)+f_1(-\xi+t)\}]$$
$$-\frac{1}{1-B_2}[f_2(\xi+t)-f_2(2-\xi+t)-B_2\{f_2(\xi+t)+f_2(2-\xi+t)\}]=Q_\xi(t). \tag{4-18}$$

These equations will determine the forms of the function f_1 and f_2 when $Q_\xi(t)$ is given.

Let us now examine the case when $Q_\xi(t)$ is the periodic exponential function of time, and put

$$Q_\xi(t)=\Omega(\xi)\exp(st), \tag{4-19}$$

where $\Omega(\xi)$ is a complex function of the parameter ξ, and s is the complex frequency. Then both f_1 and f_2 should become the exponential function of time with the same frequency s. Then we put

$$\begin{aligned} f_1&=c_1\exp(st)\\ f_2&=c_2\exp(st), \end{aligned} \tag{4-20}$$

where c_1 and c_2 are complex constants. Substituting this into Eqs. (4-17) and (4-18), and solving for c_1 and c_2, the solutions are found to be

$$c_1=\frac{1-B_1}{2}\frac{\cosh s(1-\xi)+B_2\sinh s(1-\xi)}{(1-B_1B_2)\sinh s+(B_2-B_1)\cosh s}\cdot\Omega(\xi), \tag{4-21}$$

$$c_2=\frac{1-B_2}{2}\frac{\cosh s\xi-B_1\sinh s\xi}{(1-B_1B_2)\sinh s+(B_2-B_1)\cosh s}\cdot e^{-s}\Omega(\xi). \tag{4-22}$$

Equation (4-20) with c_1 and c_2 given by the above equations is substituted into Eqs. (4-8), (4-9), (4-12), and (4-13), and we finally obtain

$$p_1'(x, t|\xi)=\frac{\cosh s(1-\xi)+B_2\sinh s(1-\xi)}{(1-B_1B_2)\sinh s+(B_2-B_1)\cosh s}(\cosh sx - B_1\sinh sx)\Omega(\xi)e^{st}, \tag{4-23}$$

$$u_1'(x, t|\xi)=-\frac{1}{\gamma}\frac{\cosh s(1-\xi)+B_2\sinh s(1-\xi)}{(1-B_1B_2)\sinh s+(B_2-B_1)\cosh s}(\sinh sx - B_1\cosh sx)\Omega(\xi)e^{st}, \tag{4-24}$$

$$p_2'(x, t|\xi)=\frac{\cosh s\xi-B_1\sinh s\xi}{(1-B_1B_2)\sinh s+(B_2-B_1)\cosh s}\{\cosh s(1-x) + B_2\sinh s(1-x)\}\Omega(\xi)e^{st}, \tag{4-25}$$

$$u_2'(x, t|\xi)=\frac{1}{\gamma}\frac{\cosh s\xi-B_1\sinh s\xi}{(1-B_1B_2)\sinh s+(B_2-B_1)\cosh s}\{\sinh s(1-x) + B_2\cosh s(1-x)\}\Omega(\xi)e^{st}. \tag{4-26}$$

The solutions given by Eqs. (4-23) through (4-26) represent the pressure oscillation driven by the periodic heat release rate $Q_\xi(t)$ at the heat plane $x=\xi$. The oscillation may be considered as a kind of forced oscillation. The amplitude of the excited oscillation is directly proportional to the magnitude of the applied heat release rate. It is not difficult to show that the acoustical resonant frequency s_0 of the system is given by

$$\tanh s_0=-\frac{B_2-B_1}{1-B_1B_2}. \tag{4-27}$$

When the frequency s of the applied heat release rate coincides with the resonant frequency s_0, the amplitude of the excited oscillation becomes infinitely large.

The solutions Eqs. (4-23) through (4-26) for a concentrated heat release are the Green's functions. For the heat release $\Omega(x)e^{st}$ of arbitrary form distributed along the chamber, the corresponding solutions can be obtained in the form of the following integrals:

$$p'(x, t)=\int_0^{1.0}p'(x, t|\xi)d\xi=\int_0^x p_2'(x, t|\xi)d\xi+\int_x^{1.0}p_1'(x, t|\xi)d\xi, \tag{4-28}$$

$$u'(x, t)=\int_0^{1.0}u'(x, t|\xi)d\xi=\int_0^x u_2'(x, t|\xi)d\xi+\int_x^{1.0}u_1'(x, t|\xi)d\xi. \tag{4-29}$$

4-3. *Initiation of Self-Excited Oscillation*

Equations (4-28) and (4-29) represent the behavior of the system when a periodic heat release is applied. The heat release rate was given as a known function of time and position, and the solutions are not sufficient to examine the instability of the system induced by combustion. In the latter case, the heat release rate can not be given as the known function, but it may vary in response to any disturbances in the system. The induced oscillation is a self-excited oscillation. In order to analyze such an instability, it is necessary to know the way of response of heat release rate q' to disturbances in the flow field. In the present analysis, this descrip-

tion of flame response to flow disturbances will be made empirically on the basis of the experimental findings.

The previous experimental studies [4] have elucidated that the increase in the heat release rate is provided as the result of spontaneous ignitions of the unburnt propellant volumes thrown out in the hot combustion gas stream by flame tip breaking. The latter, after all, is caused by the pressure decrease at the injector end of the chamber as the result of the standing pressure oscillation in the chamber. Therefore, it can be said that the pressure decrease at the injector end will produce the increase in heat release rate at the flame zone. The effect of the pressure decrease is not instantaneous, but the heat release rate will increase only after some time delay corresponding to the response time delay of the propellant.

The above suggested mechanism of the heat release rate variation is the one for the fully developed oscillation, while the present analysis is concerned with the incipient instability. As was already mentioned in the previous paper [4], however, the same mechanism may be considered to hold for the incipient state, although the variation in heat release rate in the latter case will be the smooth sinusoidal one instead of the intermittent increase. The response time delay of the propellant can be regarded as the time elapsed from the instant of the minimum pressure at the injector end till the instant of the maximum heat release rate at the flame zone. The time delay depends chiefly upon the chemical nature of the propellant and is independent of the frequency of the oscillation. It is also insensitive to the flow disturbances. The width of the flame zone, where the variation in heat release rate occurs, may be considered to be so small that it can be neglected as compared to the length of the combustion chamber.

In the hypothetical system of the present analysis, the heat release rate q' varies sinusoidally against time at the plane heat source located at $x=\xi$, in response to the sinusoidal pressure variation at $x=0$ with a constant time delay of τ^*. The latter is made nondimensional by the reference time t_0^* and is denoted as τ. For the small perturbation of heat release rate, the magnitude can be assumed to be proportional to the magnitude of the pressure perturbation at $x=0$. With these assumptions, q' can be given as

$$q'=-A\sigma_1(0)\exp s(t-\tau)\cdot\delta(x-\xi), \tag{4-30}$$

where A is the proportional constant which may be called the interaction index. The function $\sigma(x)$ is the time independent part of the pressure perturbation and is defined by the following equation.

$$p'(x,\ t)=\sigma(x)\exp(st). \tag{4-31}$$

Since the heat release rate, as well as the pressure, is the periodic exponential function of time, we can make use of the solution given by Eq. (4-23). Substituting

$$\Omega(\xi)=-A\sigma_1(0)\exp(-s\tau) \tag{4-32}$$

into the right hand side, and Eq. (4-31) into the left hand side of Eq. (4-23), we obtain

$$A\{\cosh s(1-\xi)+B_2\sinh s(1-\xi)\}+e^{s\tau}\{(1-B_1B_2)\sinh s+(B_2-B_1)\cosh s\}=0. \tag{4-33}$$

Equation (4-33) is the characteristic equation which determines the complex frequency $s=\alpha+i\beta$ as the function of the interaction index A, the plane heat source position ξ, the response time delay τ, and the specific admittance ratios B_1 and B_2. Since the real part α represents the amplification rate of the perturbation, the incipient stability of the system can be determined by solving this equation.

Although the characteristic equation (4-33) is sufficient for the purpose of the present analysis, two other cases of the flame response to flow perturbations will be examined as the additional examples of the present method. When the heat release rate at the plane heat source increases with the increase of temperature, and hence of pressure, at that position, as is the case of the Arrhenius type rate function, q' is given by

$$q'=A\sigma_1(\xi)\exp s(t-\tau)\cdot\delta(x-\xi). \tag{4-34}$$

The characteristic equation in this case becomes

$$\begin{aligned}A(\cosh s\xi-B_1\sinh s\xi)\{\cosh s(1-\xi)+B_2\sinh s(1-\xi)\}\\ -e^{s\tau}\{(1-B_1B_2)\sinh s+(B_2-B_1)\cosh s\}=0.\end{aligned} \tag{4-35}$$

When the variation in heat release rate is caused by the change of flame front area as the result of the velocity variation at the flame position, q' is given by

$$q'=\gamma A\nu_1(\xi)\exp s(t-\tau)\cdot\delta(x-\xi), \tag{4-36}$$

where $\nu(x)$ is the time independent part of the velocity perturbation and is defined by the following equation.

$$u'(x,\ t)=\nu(x)\exp(st). \tag{4-37}$$

The characteristic equation in this case becomes

$$\begin{aligned}A(\sinh s\xi-B_1\cosh s\xi)\{\cosh s(1-\xi)+B_2\sinh s(1-\xi)\}\\ +e^{s\tau}\{(1-B_1B_2)\sinh s+(B_2-B_1)\cosh s\}=0.\end{aligned} \tag{4-38}$$

If we put $A=0$ in the above three characteristic equations, they give the same solution

$$s=\tanh^{-1}\left\{-\frac{B_2-B_1}{1-B_1B_2}\right\}. \tag{4-39}$$

The obtained frequency is equal to the acoustical resonant frequency s_0 of the system. For the reasonable complex values of B_1 and B_2, the real part α becomes negative and the imaginary part β takes the value which is slightly less than the acoustical resonant frequency in the organ pipe closed at both ends. The latter equals, in the present nondimensional system, to $n\pi$ where n is the positive integer designating the order of successive higher harmonic modes of oscillation. Since

there is no energy input in the system, the flow disturbances will damp exponentially against time with the acoustical resonant frequency. Especially when $B_1=B_2=0$, α and β become zero and $n\pi$, respectively, resulting in the acoustical neutral oscillation with no energy input nor losses.

5. Numerical Calculation

5-1. *Instability Boundary*

The incipient stability of the hypothetical system for the postulated flame response can be examined by solving numerically the characteristic equation (4-33). In often cases, the reflection of pressure waves at the injector can be considered to be perfect, and hence we shall consider only the case when $B_1=0$. The critical condition for the instability of the system can be obtained by letting the real part α of the complex frequency s equal zero in the characteristic equation. After separating the real and the imaginary parts, the following two real equations are obtained.

$$A^2-B_2^2=(1-B_2^2)\{A^2\sin^2\omega(1-\xi)+\sin^2\omega\}, \tag{5-1}$$

$$\tan\omega\tau_c=\frac{B_2^2\cos\omega\cdot\sin\omega(1-\xi)-\sin\omega\cdot\cos\omega(1-\xi)}{B_2\cos\omega\xi}, \tag{5-2}$$

where ω and τ_c are the critical values of the frequency β and the response time delay τ, respectively, corresponding to the neutral oscillation. We can make use of these equations to obtain ω and τ_c as the function of A, B_2, and ξ, and thus determine the unstable ranges of the frequency β and the response time delay τ. Figure 2 presents the deviation of the critical frequency ω from the acoustic organ pipe frequency $n\pi$ as the function of A for three representative values of B_2 when $\xi=0$. The magnitude of deviation, in this case, is the same for the fundamental-mode ($n=1$), the second harmonic-mode ($n=2$), the third harmonic-mode ($n=3$),

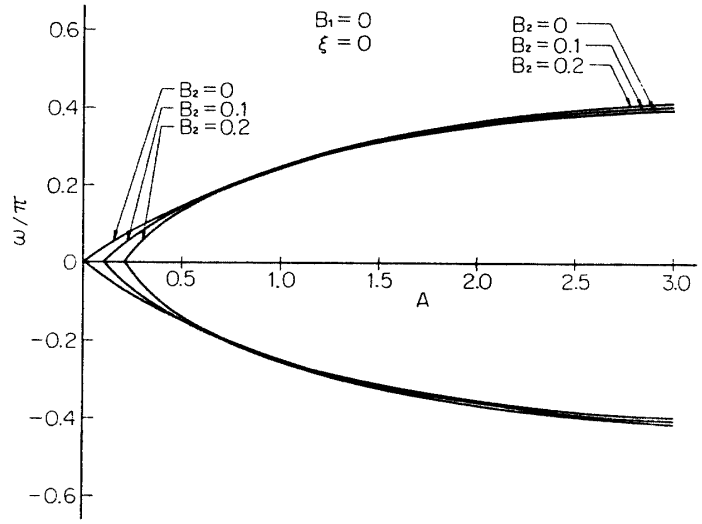

Fig. 2. Unstable ranges of nondimensional frequency as the function of interaction index for $B_1=0$, $\xi=0$.

and for any other higher harmonic-mode oscillations. As is seen in the figure, the unstable range increases with the increase of A. When $B_2 \neq 0$, the system becomes unstable only when A is larger than B_2. Figure 3 shows the corresponding unstable region of the response time delay for the first three modes of oscillation. Although for each mode of oscillation there appear repeatedly successive higher unstable regions, only the lowest unstable region is shown in the figure. This selection is based on the physical consideration that the response time delay which is longer than the oscillation period will not play any important role in the excitation of the oscillation. The figure indicates that the unstable region expands with the increase of A, while it becomes smaller with the increase of B_2. It should be noticed that there exist the regions where several modes become unstable simultaneously.

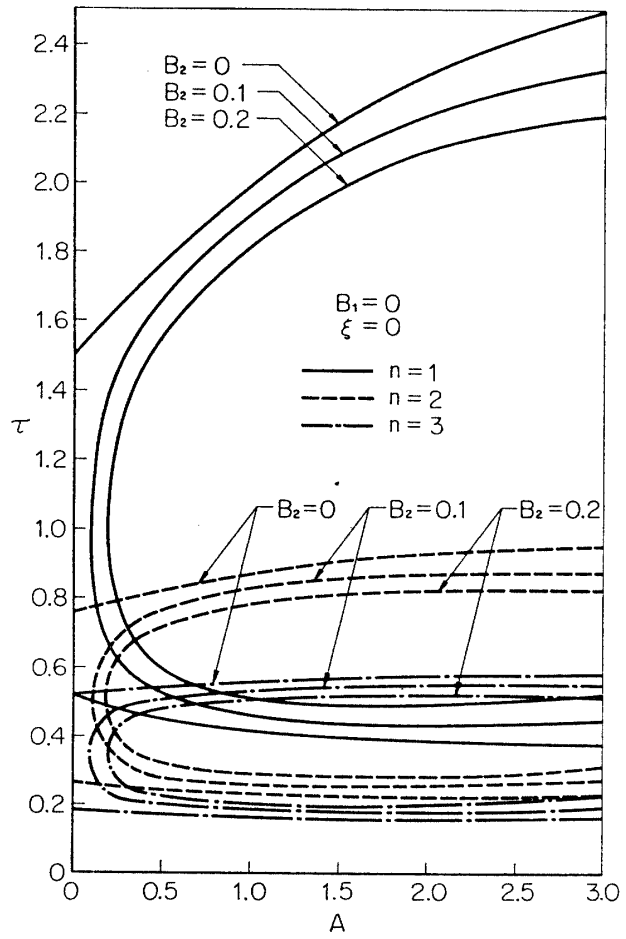

FIG. 3. Unstable ranges of nondimensional response time delay as the function of interaction index for $B_1=0$, $\xi=0$.

Figures 4~6 present the unstable range of the frequency as the function of ξ with B_2 as a parameter for the first three modes of oscillation when $A=0.5$. It can be seen that the unstable range decreases with the increase of B_2. The plane heat source position with a larger unstable range may be considered to be more likely to become unstable. As is seen in the figures the antinodal positions of the acoustic

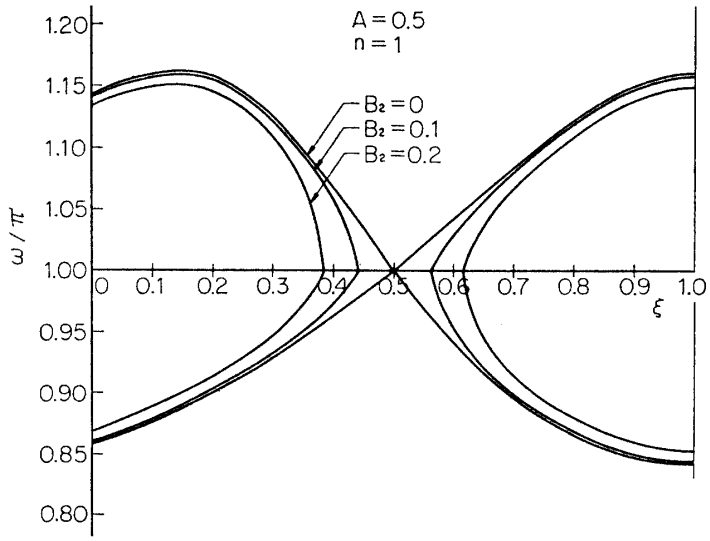

FIG. 4. Unstable ranges of nondimensional frequency as the function of nondimensional position of plane heat source for $A=0.5$. Fundamental mode.

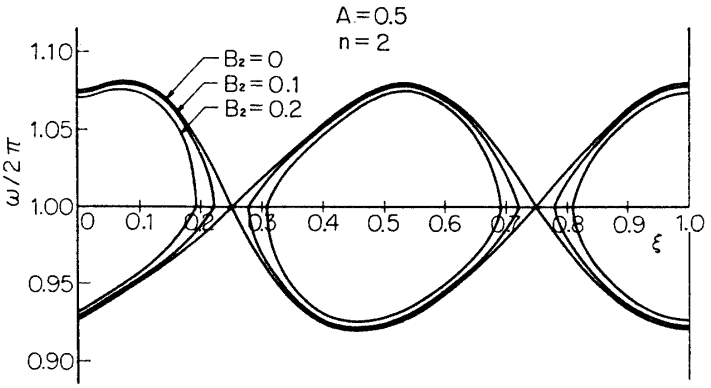

FIG. 5. Unstable ranges of nondimensional frequency as the function of nondimensional position of plane heat source for $A=0.5$. Second mode.

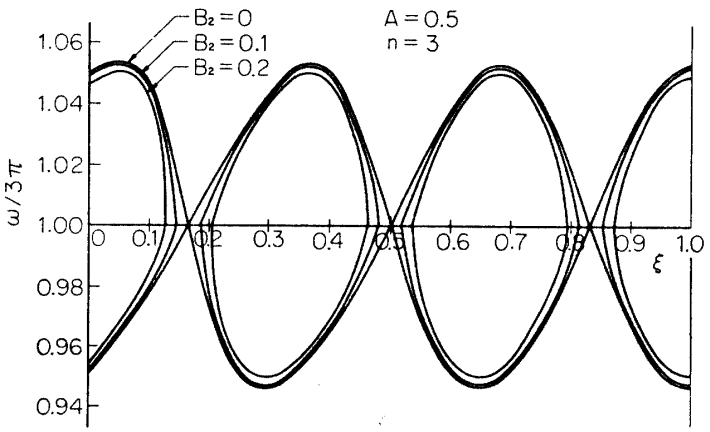

FIG. 6. Unstable ranges of nondimensional frequency as the function of nondimensional position of plane heat source for $A=0.5$. Third mode.

standing pressure oscillation are, on the whole, most unstable while the nodal positions are always most stable. Figure 7 shows the corresponding unstable region of the response time delay. The unstable region, just in the same way as that of the frequency, becomes smaller with the increase of B_2. The antinodal positions are most unstable while the nodal positions are most stable.

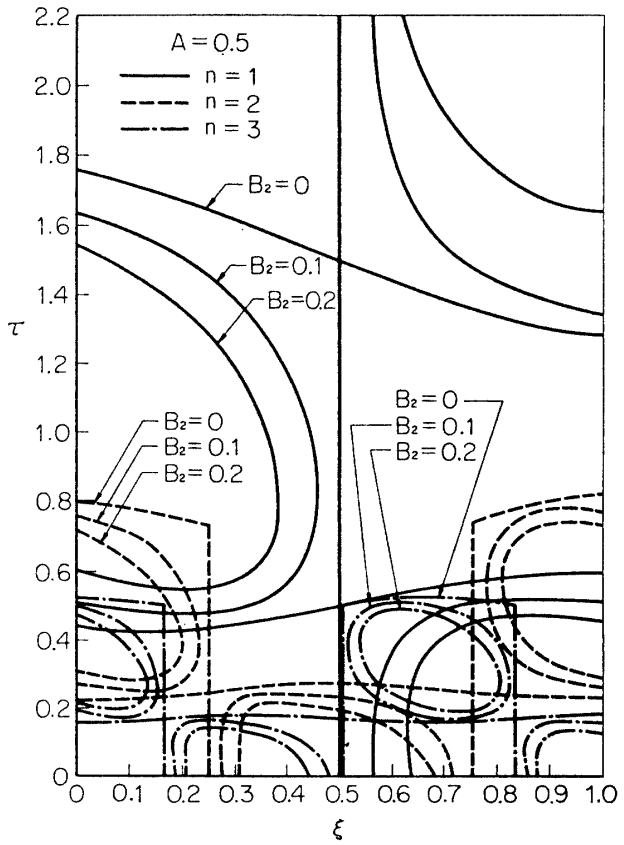

FIG. 7. Unstable ranges of nondimensional response time delay as the function of nondimensional position of plane heat source for $A=0.5$.

The critical value τ_c of the response time delay depends upon the values of A, ξ and n as well as upon that of B_2. The critical value of the frequency ω, and hence of the dimensionless oscillation period T_c, also depends upon these parameters. However, when $B_2=0$ it is not difficult to show with the use of Eq. (5-2) that there exists a unique simple relation between τ_c and T_c. The relation is given by

$$\tau_{ce}=\frac{4m+1}{4}T_c, \qquad \tau_{c0}=\frac{4m+3}{4}T_c, \tag{5-3}$$

where m is the zero or positive integer indicating the number of oscillation periods that are contained in the critical time delay τ_c. Subscript $_e$ denotes the value for the case when $\sin\omega\tau_c=1$, while subscript $_0$ denotes that for the case when $\sin\omega\tau_c=-1$. As was mentioned before, only the case of $m=0$ is considered in the present

analysis. Therefore, when the dimensional quantities are used the condition for the system to become unstable is given as

$$\frac{1}{4}T^*<\tau^*<\frac{3}{4}T^*. \tag{5-4}$$

This inequality states that each mode of oscillation is excited only when the response time delay lies between a quarter and three quarters of the oscillation period. Figure 8 shows the phase relation between the pressure and the heat release rate variation at the critical condition.

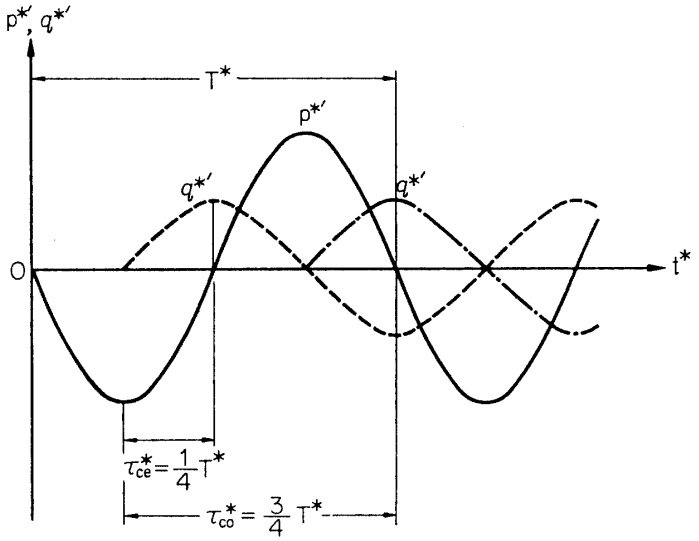

FIG. 8. Phase relation between pressure and heat release rate variation at critical conditions.

5-2. *Amplification Rate and Frequency*

The real part α of the complex frequency s gives the amplification rate or the damping rate of the perturbation, while the imaginary part β gives the frequency of the excited or the damped oscillation. In the present analysis, the characteristic equation (4-33) was solved numerically for the case when $A=0.5$, $B_2=0$, and α and β were calculated as the function of τ and ξ. Figures 9~11 present the examples of the calculated values of α [5] for the first three modes as the function of ξ with τ as a parameter. It can be seen that α is zero for any value of τ when the position of the plane heat source coincides with the nodal position of each mode oscillation. As the plane heat source goes away from the nodal position and approaches to the antinodal position, α increases or decreases gradually. However, α is not always maximum or minimum at the antinodal position. The position of the maximum amplification rate, as well as that of the maximum damping rate, depends upon the value of response time delay. Figures 12~14 present the calculated values of β for the first three modes as the function of ξ with τ as a parameter. When the position of plane heat source coincides with the nodal position, the frequency of the oscillation becomes that of the acoustic organ pipe oscillation. As

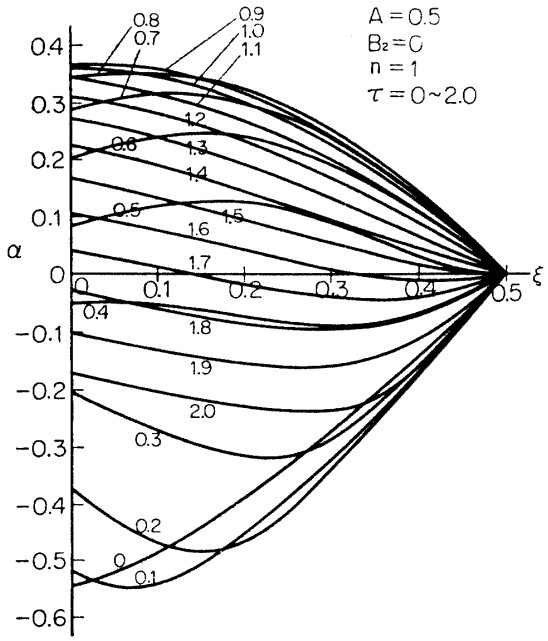

FIG. 9. Calculated nondimensional amplification rate vs nondimensional position of plane heat source for $A=0.5$, $B_2=0$. Fundamental mode.

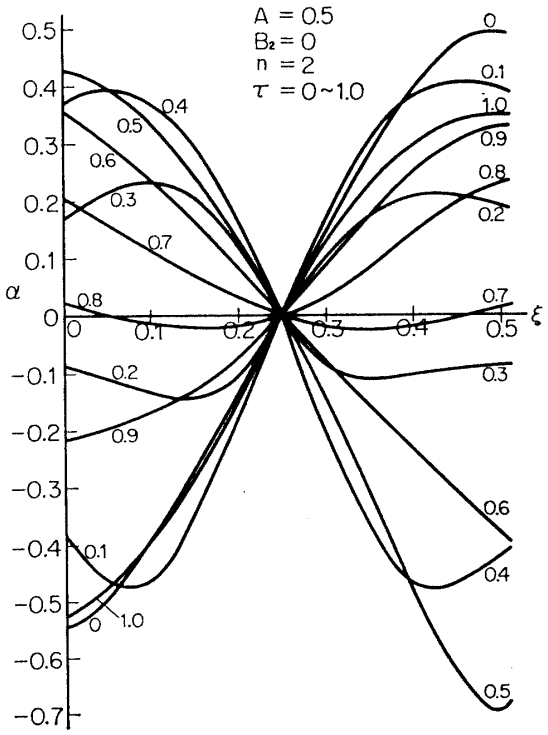

FIG. 10. Calculated nondimensional amplification rate vs nondimensional position of plane heat source for $A=0.5$, $B_2=0$. Second mode.

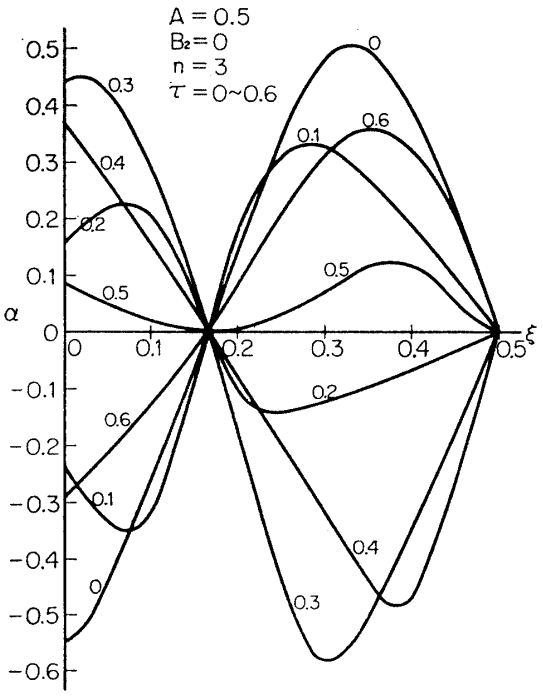

FIG. 11. Calculated nondimensional amplification rate vs nondimensional position of plane heat source for $A=0.5$, $B_2=0$. Third mode.

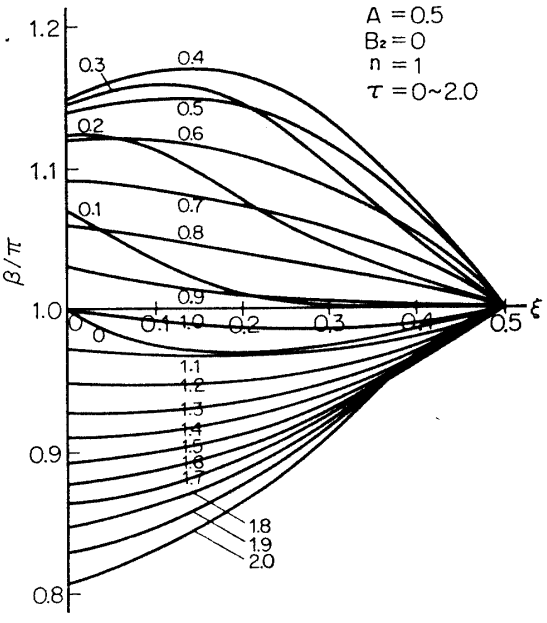

FIG. 12. Calculated nondimensional frequency vs nondimensional position of plane heat source for $A=0.5$, $B_2=0$. Fundamental mode.

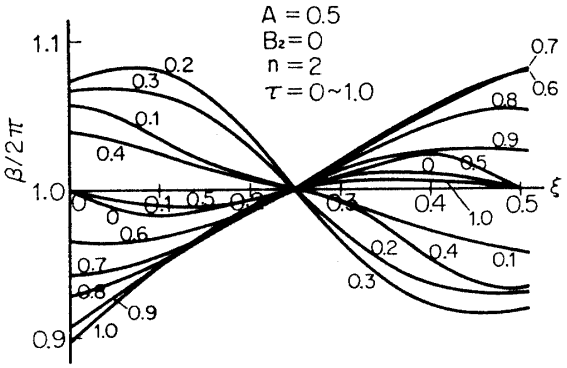

FIG. 13. Calculated nondimensional frequency vs nondimensional position of plane heat source for $A=0.5$, $B_2=0$. Second mode.

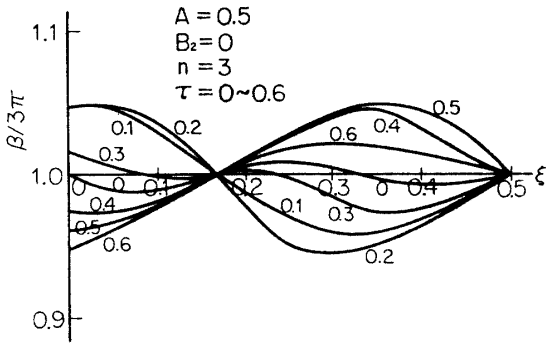

FIG. 14. Calculated nondimensional frequency vs nondimensional position of plane heat source for $A=0.5$, $B_2=0$. Third mode.

the plane heat source goes away from the nodal position and approaches to the antinodal position, the frequency deviates from that of the acoustic oscillation. However, the deviation is not always maximum at the antinodal position. The position of maximum deviation depends upon the value of response time delay.

Figure 15 presents α as the function of τ for the representative plane heat source position of $\xi=0$. When τ is increased from zero, α for each mode of oscillation first increases until it gets the maximum, and then decreases monotonously. The value of τ for the maximum value of α corresponds approximately to one half of the acoustic organ pipe oscillation period. The latter, in the present nondimensional system, equals to $2/n$, where n is the positive integer designating the mode number of the oscillation. Reference to Fig. 8 .indicates that the system is most unstable when the heat release variation is exactly in phase with the pressure variation, while it is most stable when they are out of phase with each other. For each mode of oscillation there exists one unstable range of α, where α becomes positive. The

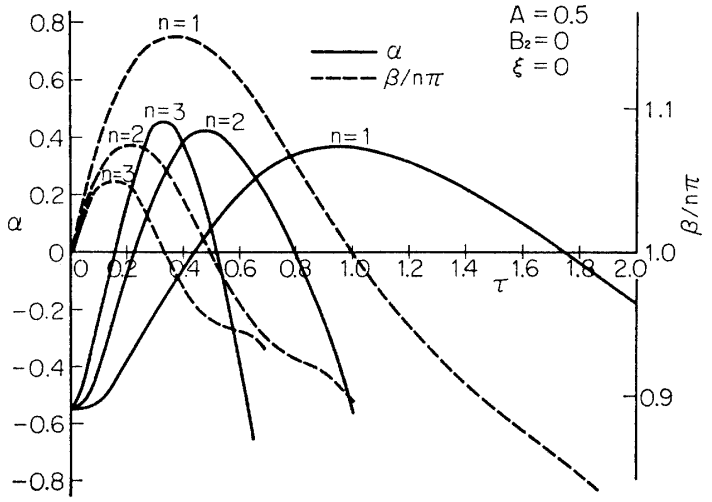

FIG. 15. Calculated nondimensional amplification rate and frequency vs nondimensional response time delay for $A=0.5$, $B_2=0$, $\xi=0$.

unstable range for each mode of oscillation overlaps one another, as was already seen in Fig. 7. In those overlapped unstable ranges, there is a possibility of more than one mode of oscillation being excited simultaneously. In the actual phenomenon, however, it is the only one mode of oscillation which can be excited for a given condition, and it is the problem which of the ovelrapped modes will be excited. In Fig. 15, the corresponding deviation of the frequency of the excited or damped oscillation is also presented. It can be seen that the frequency coincides with the acoustic one when τ is zero. With the increase of τ, the deviation increases and gets the positive maximum value, and then β decreases monotonously. It should be noticed that the deviation becomes maximum for the value of τ where α becomes zero. On the other hand, the deviation becomes zero when α is maximum. This situation will become more clear by looking at Fig. 16, in which the locus of the complex frequency s in the Gauss plane when τ is varied is shown for the case when $\xi=0$. It can be seen that the neutral oscillation frequency ω is the maximum or the minimum unstable oscillation frequency.

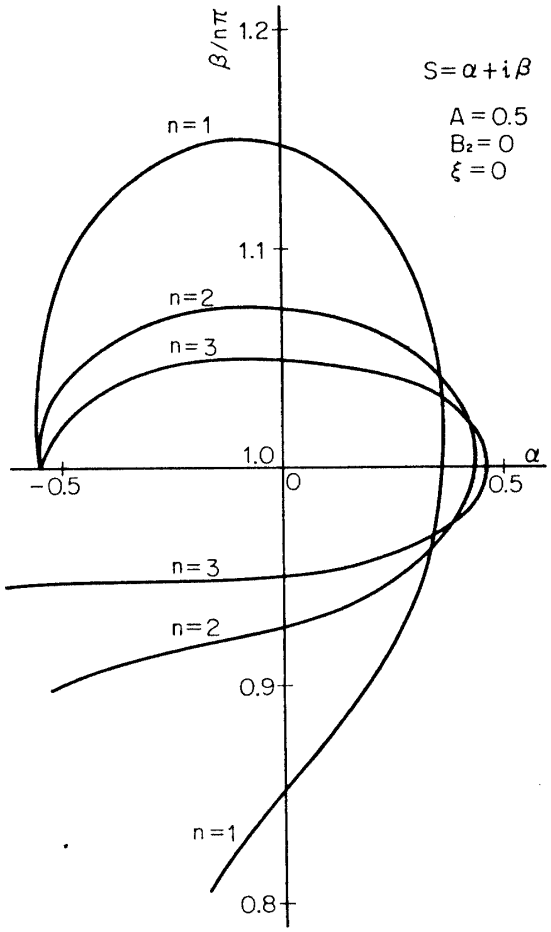

FIG. 16. Calculated nondimensional complex frequency in Gauss plane for $A=0.5$, $B_2=0$, $\xi=0$.

5-3. *Discussions of Calculated Results*

In the above numerical calculations, the solutions were obtained for the value of ξ from zero to unity. In view of the postulated driving mechanism the results will have the physical meaning, corresponding to the actual phenomenon, only for the value of ξ smaller than 0.3 or less. However, the whole result is interesting for the examination of the characteristics of the heat-driven oscillation. Figures 4~6 present the unstable ranges of the frequency as the function of the plane heat source position. These figures may be considered to represent the space condition for the excitation of the oscillation. The results shown in the figures agree generally with the space condition postulated by Rayleigh [*25*], which was already described in the previous paper [*4*]. However, the obtained results are those for the case of flame response given by Eq. (4-30), and they may be modified for the other cases of the flame response. In fact, this could be confirmed by solving the other two characteristic equations (4-35) and (4-38) for the neutral oscillation. The calculated

results for the flame response of Eq. (4-34) are quite similar to those shown in Figs. 4~6, while those of Eq. (4-36) are strikingly different. In the latter case, the antinodal position as well as the nodal position of each mode oscillation is always most stable.

The above described dependency of the space condition on the way of flame response to the flow disturbances may be interpreted as follows. In general, the space condition should depend on two different factors. The first is the dynamic effect of the heat release to amplify or damp the pressure perturbation. This effect will become more powerful as the position of heat release approaches to the antinodal position, where the amplitude of the excited pressure oscillation is maximum. At the nodal position, the pressure amplitude is zero and hence the heat release can neither drive nor damp the oscillation. The other factor is the mechanism of flame response to the flow perturbations, by which the heat release rate variation is provided. If the magnitude of heat release rate variation is proportional to the magnitude of pressure perturbation at that position, as is the case of Eq. (4-34), the provided heat release rate variation will become larger as the plane heat source approaches to the antinodal position. On the other hand, if the magnitude of heat release rate variation is proportional to the magnitude of velocity perturbation, as is the case of Eq. (4-36), the provided heat release rate variation will become smaller as the plane heat source approaches to the antinodal position of the pressure oscillation which is the nodal position for the velocity oscillation. The space condition will be determined by the combination of these two different effects. In any way, it should be noticed that the space condition for the excitation of heat-driven oscillation depends upon the way of response of heat source to the flow perturbations, and hence will be different for each individual case studied.

The unstable ranges of the response time delay shown in Fig. 7 represent the time condition for the excitation of the oscillation. As was pointed out before, when there is no energy loss, that is when $B_1=B_2=0$, the time condition is given by the simple inequality of (5-4). This inequality is essentially the same as the time criterion stated by Rayleigh [*25*]. Putnam and Dennis [*24*] gave a mathematical representation for the time criterion in the following form

$$\int_{\text{cycle}} h'p'dt>0, \tag{5-5}$$

where h' is the heat release rate, p' is the oscillating component of the pressure, and t is time. This inequality is exactly the same with that of (5-4), so long as p' and h' are the periodic exponential function of time. The inequality (5-5) holds also for the other two cases of flame response. This can easily be shown by solving the two characteristic equations for the neutral oscillation. It can be said, therefore, that the time condition is, in contrast to the space condition, independent of the mechanism of response of heat source.

The above described character of the time condition, as well as of the space condition, originates, as it happens, in the matching conditions (4-15) and (4-16) at

the plane heat source. We can make use of these conditions to show that the work done to the system by heat source in a cycle of oscillation W is given by

$$W=\int_{\text{cycle}} p_2'u_2'dt-\int_{\text{cycle}} p_1'u_1'dt$$
$$=\int_{\text{cycle}} p'(u_2'-u_1')dt=\frac{1}{\gamma}\int_{\text{cycle}} p'Q_\xi(t)dt. \tag{5-6}$$

When there is no energy loss in the system, the work done to the system W equals to the net energy input to the system. The whole of this energy input will be converted into the oscillation energy. If W is positive, therefore, the energy of oscillation is supplied and the oscillation will be excited, while the oscillation will be damped if W is negative. The excitation will be more powerful as the positive value of W is larger. Thus the conditions for the excitation of heat-driven oscillation can be proved with the use of the matching conditions at the plane heat source.

Figures 9~14 present the real part and the imaginary part of the complex frequency as the function of τ and ξ. There are number of linear theories developed so far for the occurrence of heat-driven oscillation. All of these theories are concerned only with the instability boundary and hence the characteristic equation was solved only for the neutral oscillation of $\alpha=0$. However, in the analysis it is often the case that the instability regions for several modes overlap one another. In such a case those theories can say nothing about which of the overlapped modes will be excited, and the problem has been considered to be outside the scope of the linear theory. Th method developed in the present study has brought about the relatively simple means of calculating the complex frequency of the excited or the damped oscillation. Although there still remains some question about the physical significance of the obtained amplification rate α and frequency β, the former will at least give the measure for the ability of the system being excited or damped dynamically.

The calculation of the frequency β of the excited or damped oscillation indicates that the frequency will deviate from that of the acoustic oscillation. The magnitude of the deviation depends upon the values of parameters A, B_2, ξ and τ. When the coupling between the heat source and the flow field is not so strong and hence the value of A is less than unity, the deviation is rather small and about 25% at most. It should be noticed that the deviation is maximum when there is no amplification or damping, while it is zero when the amplification or damping is most strong. This behavior of the frequency change has been stated by Rayleigh [*25*], and its physical interpretation was advanced by Wood [*26*].

6. Comparison with Experiment

6-1. *Theoretical Oscillation Boundary*

In order to confirm the validity of the present analysis, the instability boundary calculated for the hypothetical analytical system was used to obtain the condition

for occurrence of the oscillation in the actual combustion chamber. The theoretical oscillation boundary in φ (propellant equivalence ratio) $-L_c$ (combustion chamber length) plane was calculated with the use of amplification rate α calculated in the preceding section for the case when $A=0.5$ and $B_2=0$, and the result was compared with the oscillation boundary observed in the experimental studies of the present investigation. The comparison was made for the standard experimental condition of P_c (mean combustion chamber pressure) $=3.0$ kg/cm^2 abs. and M_i (propellant injection Mach number) $=0.29$, and the corresponding experimental oscillation boundary is that shown in Fig. 8 of reference [2].

The theoretical analysis in the preceding section was made in the nondimensional system, and in order to apply the result to the actual dimensional system it is necessary to fix the reference quantities. The representative length L in this case is, of course, the combustion chamber length L_c, while the injector end of the chamber, where the temperature of the combustion gas is maximum, can be taken as the reference position. The reference time t_0^* is now the time required for a sound wave to travel the chamber length L_c under the conditions corresponding to the stagnant combustion gas at the injector end. The nondimensional amplification rate α is already given as the function of $\xi=\xi^*/L_c$ and $\tau=\tau^*/t_0^*$, while the dimensional amplification rate $\alpha^*=\alpha/t_0^*$ should be known as the function of φ and L_c so as to determine the theoretical oscillation boundary. It is required, therefore, to know ξ^*, τ^* and t_0^* as the function of φ and L_c.

The plane heat source position ξ^* was assumed to correspond to the average flame tip position of tubulent multiflames. The data of temperature distribution shown in Fig. 16 of reference [4] was used to determine ξ^* as the function of φ, and the result is shown in Fig. 17. This may be thought somewhat too rough, the value of ξ^*, however, is not crucial in the present calculation. As to the response time delay, an important assumption was introduced. The analysis in the preced-

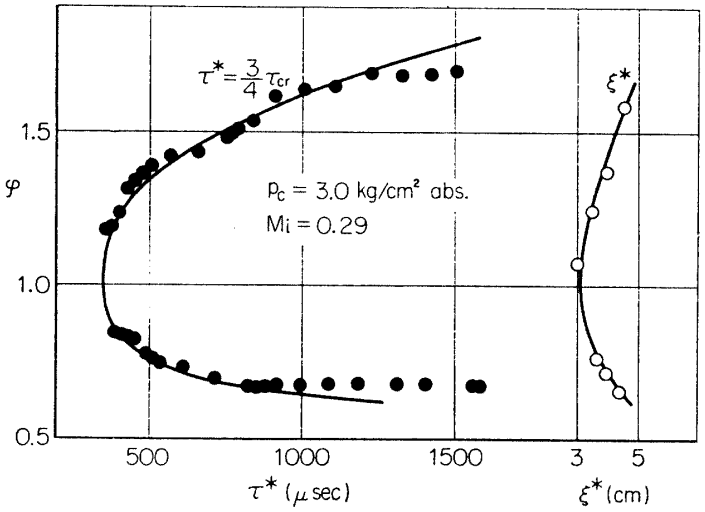

FIG. 17. Response time delay and plane heat source position vs propellant equivalence ratio for $P_c=3.0$ kg/cm^2 abs., $M_i=0.29$.

ing section has indicated that there exists the simple relation of Eq. (5-3) between the response time delay and the oscillation period at the critical condition. It was assumed, therefore, that the response time delay τ^* is equal to three quarters of the lower critical oscillation period τ_{cr} observed in the previous experimental studies [2]. Since τ_{cr} depends only on φ for given values of P_c and M_i, τ^* is the function of φ only being independent of L_c. According to this assumption, the observed lower critical oscillation period for the fundamental-mode oscillation, shown in Fig. 9 of reference [2], was used to obtain τ^* and the result is shown in Fig. 17. The reference time $t_0^*=L_c/\bar{c}_0^*$ is the function of φ, as well as of L_c, since the combustion gas temperature and hence the sound velocity depends on φ. This dependency was determined by using the experimental data shown in Fig. 18 of reference [4] and the result is shown in Fig. 18. The figure also presents the ratio of the sound velocity for any value of φ to that for $\varphi=1.0$. The sound velocity for $\varphi=1.0$ was calculated by using the numerical values of $\bar{T}_0^*=1{,}700°\mathrm{K}$, $\gamma=1.256$ (for $\varphi=1.0$, $T=1{,}700°\mathrm{K}$), and $R^*=30.63\ \mathrm{kg\cdot m/°K\cdot kg}$ (for $\varphi=1.0$), and found as

$$\bar{c}_0^*=(\gamma g R^* \bar{T}_0^*)^{\frac{1}{2}}=801\ \mathrm{m/sec.}$$

The sound velocity for any other value of φ was obtained by multiplying the above ratio to this value. In this way, the dimensional α^* was determined as the function of φ and L_c. As was pointed out before, there exists a slight temperature gradient of the combustion gas along flow direction in the actual combustion chamber, while the gas temperature was assumed to be constant in the analysis. In calculating the theoretical oscillation boundary, therefore, the correction of the wave propagation time for this temperature gradient was made [5].

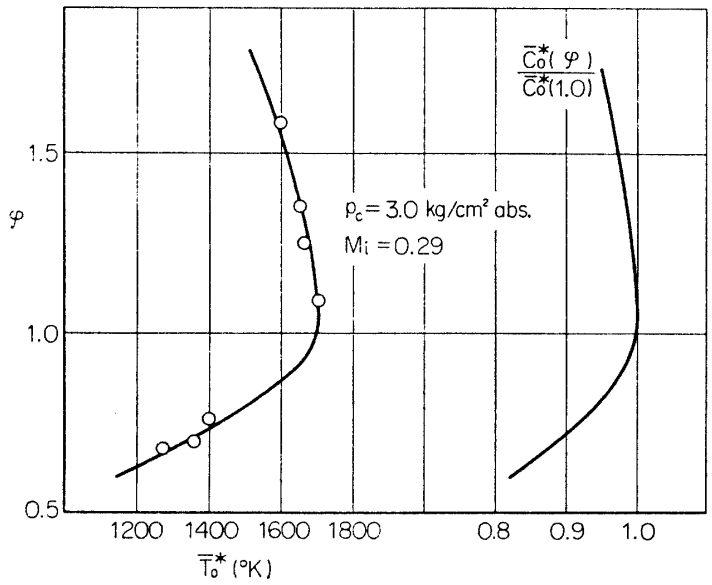

FIG. 18. Combustion gas temperature and ratio of sound velocity vs propellant equivalence ratio for $P_c=3.0\ \mathrm{kg/cm^2}$ abs., $M_i=0.29$.

Figures 19~22 present the calculated α^* as the function of φ with L_c as a parameter. In Fig, 19 it can be seen that when L_c is rather small α^* is maximum in the vicinity of $\varphi=1.0$. When L_c is increased the α^* curve progresses steadily toward positive larger value. When L_c is smaller than 16 cm, α^* is always negative for any value of φ, indicating that the disturbances will be damped dynamically and no oscillation will occur. However, when L_c is increased to 18 cm, α^* becomes positive for a certain range of φ around the stoichiometric, and the oscillation of the fundamental mode will appear in this range. With the increase of L_c, the unstable range of φ expands extending its boundary both in the rich and the lean sides. Figure 20 presents the case when L_c is varied from 30 cm to 40 cm. In this case, with the increase of L_c, α^* for the fundamental mode decreases in the vicinity of stoichiometric, while α^* for the second mode appears in the left hand side and

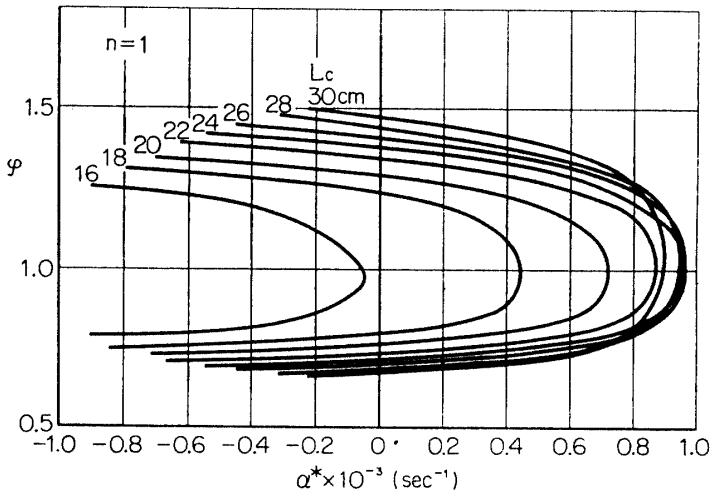

FIG. 19. Calculated amplification rate vs propellant equivalence ratio. L_c=16~30 cm.

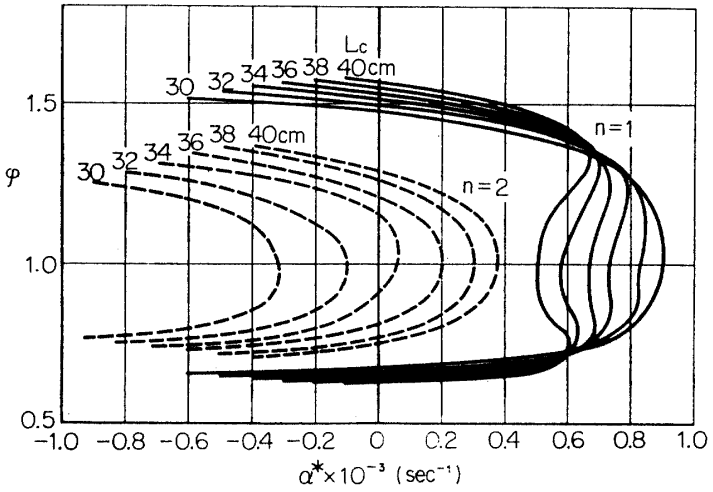

FIG. 20. Calculated amplification rate vs propellant equivalence ratio. L_c=30~40 cm.

increases just in the same way as the fundamental mode α^* in Fig. 19. When L_c is smaller than 32 cm, the second mode α^* is negative for any value of φ, indicating that the second mode oscillation will not occur. However, when L_c is increased to 34 cm, the second mode α^* becomes positive for a certain range of φ in the vicinity of stoichiometric. In this range of φ, α^* of the fundamental mode and the second mode become positive simultaneously, and the oscillation of both mode may be excited. In such a case, it is assumed in the present study that the mode with larger value of α^* only will be excited. Therefore, only the fundamental-mode oscillation will occur when L_c is smaller than 40 cm.

When L_c is increased further, the second mode α^* increases further while the fundamental mode α^* decreases near the stoichiometric, and finally the former exceeds the latter. This situation is shown in Fig. 21 which presents the cases for L_c $=50$ cm and 60 cm. In these chamber lengths, the second-mode oscillation will occur in the vicinity of stoichiometric and the fundamental-mode oscillation will occur both in the richer and the leaner sides. The third mode α^* appears in the left side

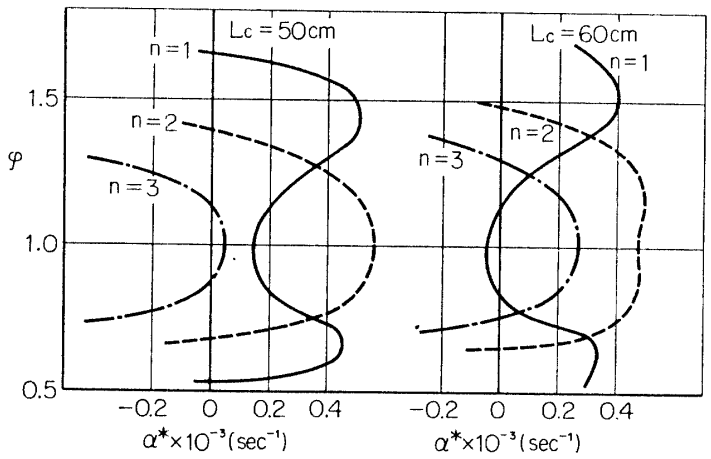

FIG. 21. Calculated amplification rate vs propellant equivalence ratio. L_c=50 and 60 cm.

but this mode oscillation does not occur in these chamber lengths. With the further increase of L_c, the unstable range of the second mode becomes larger extending its boundary both in the rich and the lean sides, while the third mode α^* increases near the stoichiometric. At the chamber length of 70 cm, the third mode α^* exceeds the second mode α^* in the vicinity of stoichiometric, and the third-mode oscillation occurs in this range of φ. Figure 22 indicates that for the longer chamber lengths the oscillation of the fundamental, the second, and the third mode will occur for each respective range of φ.

Figure 23 shows the dependency of α^* on L_c with φ as a parameter. It can be seen that for a given value of φ there exists the upper critical chamber length, as well as the lower critical chamber length, for each mode of oscillation. When the chamber length is smaller than the lower critical chamber length of the fundamental mode, α^* for any mode of oscillation is negative indicating that any disturbance will

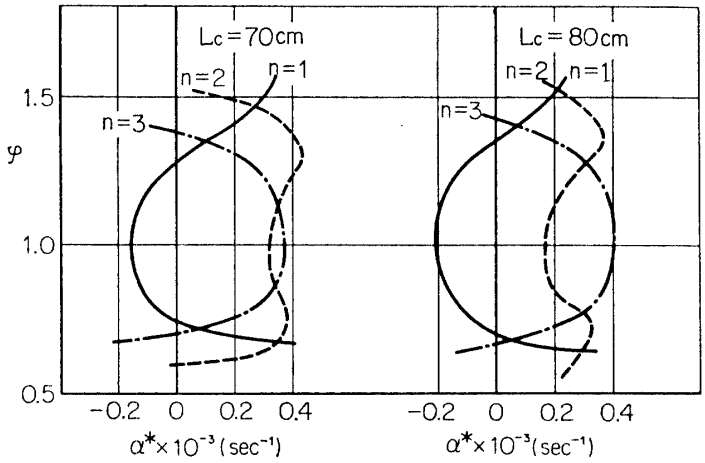

FIG. 22. Calculated amplification rate vs propellant equivalence ratio. L_c=70 and 80 cm.

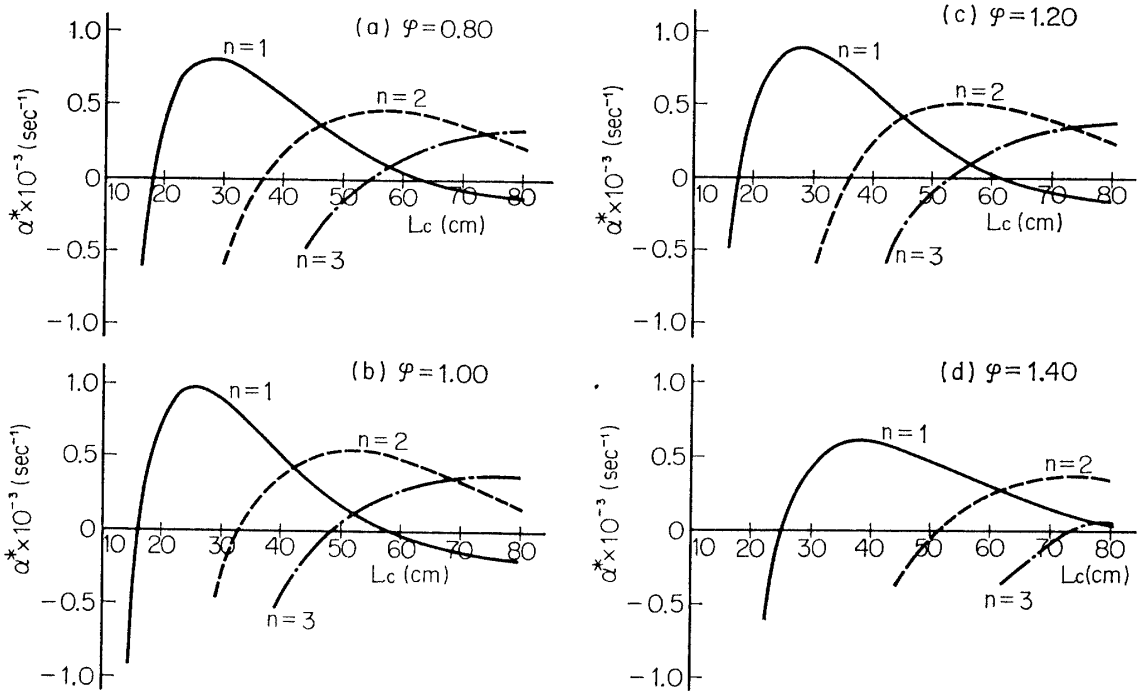

FIG. 23. Calculated amplification rate vs combustion chamber length.
(a) φ=0.80 (b) φ=1.00
(c) φ=1.20 (d) φ=1.40

be damped dynamically and no oscillation will occur. With the increase of the chamber length the fundamental-mode oscillation will first occur. With the further increase of the chamber length, the oscillations of the higher successive modes will occur one after another. It should be noticed that the increase of α^* near the lower critical chamber length for the fundamental mode is very rapid while its decrease near the upper critical chamber length is gradual. The maximum value of α^* becomes smaller for the higher mode, which suggests that the higher mode oscillation is less likely to occur even when the effect of viscosity is not taken into account.

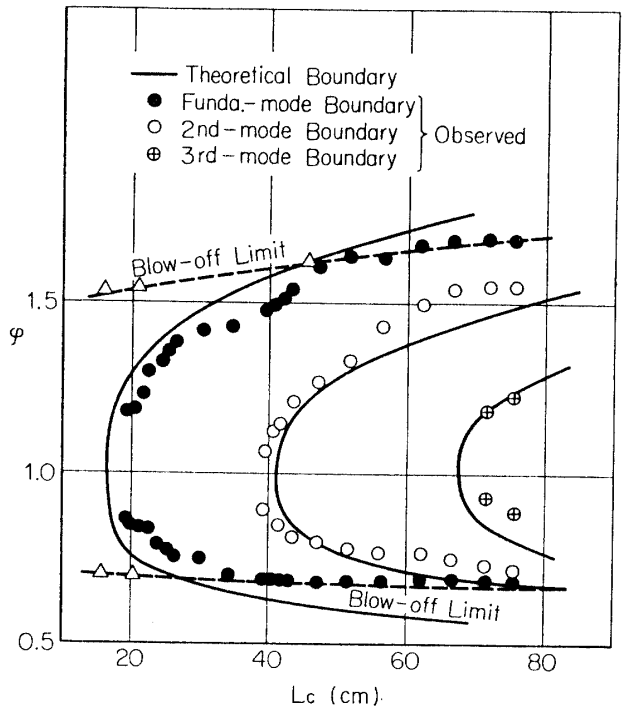

FIG. 24. Theoretical and observed oscillation boundaries in propellant equivalence ratio—combustion chamber length plane.

The above obtained results were used to determine the theoretical oscillation boundary for each mode of oscillation in $\varphi - L_c$ plane. The result is shown in Fig. 24, in which the theoretical boundaries are shown by solid curves. For the purpose of comparison, the experimentally observed boundaries are also shown by circles. The correlation between the theory and the experiment is fine.

6-2. *Discussions*

It was shown that the result of the present analysis when applied to the calculation of the theoretical oscillation boundary correlates very well with the experimental result. In the course of the calculation several assumptions were made. The most important assumption was that the response time delay of the propellant corresponds to three quarters of the lower critical oscillation period. The simple analysis in the hypothetical system of the present study can only predict the relation between the dimensionless variables, such as Eq. (5-3), which they should satisfy at the critical condition. The existence of the response time delay was assumed beforehand, and as a matter of fact the analysis can give no information about the absolute value itself of the response time delay. Therefore, when the result of the analysis is intended to apply to the actual dimensional system, the response time delay of the system has to be given. In principle, the information should be provided by some other experimental data or theories which are independent of the present analysis. Owing to a lack of the appropriate data, in the present study the value of the response time delay was determined by the aforementioned assumption, which is based on the result of the present analysis. This assumption may be justified by

the agreement of the theory with the experiment. As was pointed out in the previous paper [4], the response time delay is in substance the ignition time delay of the propellant. The data on the ignition time delay of the gasoline vapor was obtained by Zukoski and Marble [27] from the blow off experiment of the flame stabilized by the hot recirculation zone. When their data are compared with those shown in Fig. 17, it is found that two data correlate well in magnitude as well as in their dependency on the equivalence ratio.

The calculated oscillation boundaries are found to agree well with those of the experiment not only for the instability boundary of the fundamental-mode oscillation but also for the transitions from the fundamental-mode oscillation to the second-mode oscillation and from the second- to the third-mode oscillation. In the calculation of these transition boundaries it was assumed that the mode with the largest value of α^* is preferred when several modes become unstable simultaneously. This treatment may not be justified in the scope of the present linear theory. However, it should be noticed that in Figs. 19~22, α^* of each mode oscillation crosses one another rather sharply near the point of intersection. This means that in the vicinity of this point the amplification rate of one mode increases rapidly for the small change of φ while that of the other mode decreases rapidly. In such a case, it is clear that the transition of the oscillation mode should occur near the point of intersection. Therefore, there is a chance that even the linear theory can give the correct prediction. The agreement of the result with that of the experiment indicates that this is, in fact, the case.

In the calculation the specific admittance ratio B_2 of the exhaust nozzle was assumed to be zero, and hence the effect of the energy loss through the nozzle was not considered. The experimental study [28] of determining the damping rate α^* due to the energy loss with the use of cold rocket motors has indicated that its magnitude is about a tenth of the maximum value of α^* calculated in the present study. This value, when made nondimensional, corresponds approximately to the value of 0.05 for B_2. Therefore, it may be considered that the role played by the energy loss in determining the incipient instability is not so important. Perhaps, the choice of the value of the interaction index A will be more crucial. Another value of A, instead of 0.5, may bring about the better correlation with the experiment. In other words, the value of A might have been determined so that the calculated boundaries agree exactly with those of experiment. However, it is questionable if it deserves to determine such a value of A so as to get a more close agreemnet with the experiment.

The results shown in Fig. 23 offer an interesting suggestion. The amplification rate α^* of the fundamental-mode oscillation increases very rapidly near the lower critical chamber length, whereas its decrease near the upper critical chamber length is rather gradual. This means that there exists a very definite lower critical chamber length, above which the fundamental-mode oscillation occurs. This prediction of the present study well explains why in so many experiments in liquid or gaseous propellant rocket motors the existence of the lower critical chamber length has

always been observed while that of the upper critical chamber length has remained rather obscure.

7. Concluding Remarks

The agreement between the theory and the experiment confirms the validity of the initiating and driving mechanism postulated in the previous paper [*4*] for the combustion oscillation in the premixed gas rocket. The excited oscillation is a kind of heat-driven oscillation with a constant time delay. The interaction between the pressure wave and the flames which actually drives the oscillation does not depend on chemical kinetics but it depends on more complicated fluid mechanical influences, even in the relatively simple combustion system of premixed gas rocket. This interaction is so complicated that its theoretical prediction seems almost impossible. It is inevitable, therefore, that in the theoretical analysis of the combustion oscillation of this sort the mathematical representation of the interaction should become an empirical one based on the experimental finding.

In the experiments of the premixed gas rocket, the observed pressure oscillations have always been the so-called shock type oscillation with the rapid pressure increase. However, as was already pointed out repeatedly in the previous papers [*3*], [*4*],[*5*], the shock wave does not play any important role in the driving as well as in the characteristic of the oscillation. The excited oscillation is a linear instability in the sense that it develops from the amplification of small sinusoidal disturbances which can be suitably described by linear equations.

The present investigation has made clear the nature of the combustion oscillation in the premixed gas rocket. However, there arises a question what can be the significances of the above obtained results in the instability of the liquid propellant rocket. The combustion process in the liquid propellant rocket is more complicated one, and the combustion is distributed in the whole chamber. No discrete position of the combustion zone, such as the flame front position in case of the premixed gas rocket, can be designated. In this point of view, the gas rocket appears to be more representative of solid propellant rocket, rather than of liquid propellant rocket. In the instability of the solid propellant rocket also, the interaction between the pressure wave and the combustion process should be restricted to the reaction zone concentrated to the solid surface, and the propagation of the wave in the rest of the chamber may be isentropic. Although the mechanism of the interaction itself may be quite different from that of the premixed gas, if the response of heat evolution to flow disturbances can be known the present analytical method can be applied for predicting the occurrence of the oscillation.

On the other hand, the propagation of the pressure wave in the liquid propellant rocket motor with the distributed combustion zone will not be isentropic. However, the experimental observations [*29*]~[*35*] indicate that the observed frequency of the oscillation corresponds approximately to that of the fundamental acoustic mode in the combustion chamber with both ends closed, and that the finite amplitude pressure waves originate in the zone near the injector end where the combustion is most active. Therefore, it may be considered that even in the liquid propellant rocket the

interaction of pressure waves and the combustion process is important only in the restricted zone near the injector end, and the propagation of the wave in the rest of the chamber is approximately isentropic. If it is so, the similar theoretical treatment will be possible for the study of the linear instability in the liquid propellant rocket also. The details of the interaction, of course, will be different from that of the premixed gas rocket. However, the existence of the definite lower critical chamber length for the liquid propellant rocket suggests that the interaction should be related to some phenomenon which presents a characteristic time. The generalized wave equation derived in the present study reveals the close correlation between the pressure increase and the heat release. The finite pressure wave with a very rapid pressure increase, which is observed in so many experiments of the liquid propellant rocket, must be accompanied by a powerful instantaneous heat release in the reaction zone. Such an instantaneous heat input is only possible by the spontaneous ignition of the unburnt combustible mixture. Although the details of the interaction phenomena in the liquid propellant rocket must be made clear through the carefully organized experimental works, more attention may be directed to the spontaneous ignition.

Acknowledgement

The author would like to express his sincere thanks to Professor H. Tsuji for his helpful guidance and counsel throughout the course of the present study.

Department of Jet Propulsion,
Institute of Space and Aeronautical Science,
University of Tokyo, Tokyo
September 25, 1968

References

[1] Tsuji, H. and Takeno, T.: "Studies of High Frequency Combustion Oscillations in a Gaseous Propellant Rocket Motor", Aero. Res. Inst., Univ. of Tokyo, Report No. 391 (1964).

[2] Tsuji, H. and Takeno, T.: "An Experimental Investigation on High-Frequency Combustion Oscillations", Tenth Intern. Symp. on Combustion, Combustion Institute, Pittsburgh (1965), p. 1327.

[3] Tsuji, H. and Takeno, T.: "Propagation of Pressure Wave in High-Frequency Combustion Oscillation", AIAA Journal, vol. 6 (1968) p. 730.

[4] Takeno, T.: "Experimental Studies on Driving Mechanism of the High Frequency Combustion Oscillation in a Premixed Gas Rocket", ISAS Report No. 420 (1968).

[5] Takeno, T.: "An Investigation on High Frequency Combustion Oscillation in Premixed Gas Rocket", Doctor Thesis, Graduate School of Aero. Eng., Univ. of Tokyo (1967).

[6] Sirignano, W. A. and Crocco, L.: "A Shock Wave Model of Unstable Rocket Combustors", AIAA Journal, vol. 2 (1964), p. 1285.

[7] Culick, F. E. C.: "Stability of High Frequency Pressure Oscillations in Rocket Combustion Chambers", AIAA Journal, vol. 1 (1963), p. 1097.

[8] Murthy, S. N. B. and Osborn, J. R.: "Stability Criteria for Longitudinal Pressure Oscillations in a Rocket Motor", Journ. Acous. Soc. America, vol. 37 (1965), p. 872.

[9] Crocco, L and Cheng, S. I.: "High Frequency Combustion Instability in Liquid Propellant Rocket Motors", AGARDOGRAPH No. 8, Butterworths Scientific Publications, London (1956).

[10] Blackshear, P. L., Jr.: "Driving Standing Waves by Heat Addition", NACA TN 2772, August 1952.

[*11*] Blackshear, P. L., Jr.: "Driving Standing Waves by Heat Addition", Fourth Intern. Symp. on Combustion, Williams and Wilkins Co., Baltimore (1953), p. 553.
[*12*] Bailey, J. J.: "A Study of Flame-Excited Oscillation in a Tube", Journ. Appl. Mech., September 1957, p. 333.
[*13*] Merk, H. J.: "Analysis of Heat-Driven Oscillations of Gas Flows, I. General Considerations", Appl. Sci. Res. A vol. 6 (1956–57), p. 317.
[*14*] Merk, H. J.: "Analysis of Heat-Driven Oscillations of Gas Flows, III. Characteristic Equation for Flame-Driven Oscillations of the Organ-Pipe Type", Appl. Sci. Res. A vol. 7 (1957–58), p. 175.
[*15*] Merk, H. J.: "Analysis of Heat-Driven Oscillations of Gas Flows, IV. Discussion of the Theoretical Results concerning Flame-Driven Oscillations", Appl. Sci. Res. A Vol. 7 (1957–58), p. 192.
[*16*] Merk, H. J.: "Analysis of Heat-Driven Oscillations of Gas Flows, V. Influence of Heat Transfer in the Burner Ports on the Stability of Combustion of Premixed Gases", Appl. Sci. Res. A vol. 8 (1958–59), p. 1.
[*17*] Merk, H. J.: "An Analysis of Unstable Combustion of Premixed Gases", Sixth Intern. Symp. on Combustion, Reinhold Publishing Corp., New York (1957), p. 500.
[*18*] Markstein, G. H.: "Perturbation Analysis of Stability and Response of Plane Flame Fronts", "Experimental Studies of Flame-Front Instability", Nonsteady Flame Propagation, Pergamon Press, New York (1964), p. 15, p. 75.
[*19*] Chu, B. T.: "On the Generation of Pressure Waves at a Plane Flame Front", Fourth Intern. Symp. on Combustion, Williams and Wilkins Co., Baltimore (1953), p. 603
[*20*] Chu, B. T.: "Pressure Waves Generated by Addition of Heat in a Gaseous Medium", NACA TN 3411, June 1955.
[*21*] Chu, B. T.: "Mechanism of the Generation of Pressure Waves at Flame Fronts", NACA TN 3683, October 1956.
[*22*] Ruddinger, G.: "Shock Wave and Flame Interactions", Combustion and Propulsion, Pergamon Press, London (1958), p. 153.
[*23*] Williams, F. A.: "Combustion Theory", Addison-Wesley Publishing Co., London (1965).
[*24*] Putnam, A. A. and Dennis, W. R.: "Burner Oscillations of the Gauze-Tone Type", Journ. Acous. Soc. America, vol. 26 (1954), p. 716.
[*25*] Rayleigh, L.: "Theory of Sound", vol. II, Dover Press, New York (1945), p. 226.
[*26*] Wood, A.: "Acoustics", Interscience (1941), p. 93.
[*27*] Zukoski, E. E. and Marble, F. E.: "Experiments concerning the Mechanism of Flame Blowoff from Bluff Bodies", Proceedings of the Gas Dynamics Symposium on Aerothermochemistry, Northwestern University, Evanston (1956), p. 205.
[*28*] Buffum, F. G. Jr., Dehority, G. L., Slates, R. O. and Price, E. W.: "Acoustic Attenuation Experiments on Subscale, Cold-Flow Rocket Motors", AIAA Journal, vol. 5 (1967), p. 272.
[*29*] Berman, K. and Logan, S. E.: "Combustion Studies with a Rocket Motor Having a Full-Length Observation Window", Journ. American Rocket Soc., vol. 22 (1952), p. 78.
[*30*] Berman, K. and Cheney, S. H. Jr.: "Combustion Studies in Rocket Motors", Journ. American Rocket Soc., vol. 23 (1953), p. 89.
[*31*] Berman, K. and Cheney, S. H. Jr.: "Rocket Motor Instability Studies", JET PROPULSION, vol. 25 (1955), p. 513.
[*32*] Ellis, H., Odgers, I., Stosick, A. J., Van de Verg, N. and Wick, R. S.: "Experimental Investigation of Combustion Instability in Rocket Motors", Fourth Intern. Symp. on Combustion, Williams and Wilkins Co., Baltimore (1953), p. 880.
[*33*] Tischler, A. O., Massa, R. V. and Mantler, R. L.: "An Investigation of High Frequency Combustion Oscillations in Liquid-Propellant Rocket Engines", NACA RM E53B27, June 1953.
[*34*] Ross, C. C. and Datner, P. P.: "Combustion Instability in Liquid Propellant Rocket Motors—A Survey", Selected Combustion Problems, Butterworths Scientific Publications, London (1954), p. 352.
[*35*] Barrere, M.: "Combustion Instability in Liquid-Propellant Rocket Motors", Rocket Propulsion, Elsevier Publishing Co., Amsterdam (1960), p. 646.